A Comparative Analysis of Remote Sensing Methods for Burn-Scar Mapping in Wetlands

Looking north over Monkeygar Creek and Gibson Way towards the Northern Marshes. July, 2017.

Mackenzie Austin
Department of Environmental Sciences
Faculty of Science and Engineering
Macquarie University
Submission Date: 09/10/17

Declaration

I hereby state that the body of this thesis, prepared for submission for the degree of Masters of Research, is of no more than 20,000 words (excluding tables and captions) and 50 pages of text (excluding front matter, references, and appendices).

Except where otherwise stated, the work contained within this document is wholly of my own efforts.

Mackenzie Austin

Date: 09/10/17

Table of Contents

Declaration ii

Table of Contents iii

List of Figures iv

List of Tables v

List of Equations v

List of Appendices v

Acronyms and Definitions vi

Acknowledgements vii

Thesis Abstract viii

1. Preface 1

1.1 Introduction and Relevance 1

1.2 Previous Research on Remote Sensing Based Land Cover Analysis 3

2. Journal Paper 16

2.1 Abstract 16

2.2 Introduction 16

2.3 Methods 18

2.4 Results and Analysis 28

2.5 Evaluation and Conclusion 46

3. Synthesis 49

3.1 Future Research Directions 49

References 51

Appendix 59

List of Figures

Figure 1: False colour infrared view of Macquarie Marshes wetland with fire boundary overlay before and after a fire……..……..4

Figure 2: Comparison between NDVI (top) and NBRI (bottom) pre-fire (left) and post-fire (right). Background imagery is false colour NIR……...11

Figure 3: Macquarie Marshes wetland at one week post-fire (Left) and the same area at three weeks post-fire (Right). Image credit Peter Berney, Office of Environment and Heritage (OEH), NSW.....17

Figure 4: Map of study area and fire events. Imagery © Land and Property information (LPI), 2015……...…….19

Figure 5: Map of vegetation communities for study area. Data from OEH (2013). Imagery © Land and Property information (LPI), 2015……....21

Figure 6: Comparison of post-fire EVI2 mean index value change over time……..33

Figure 7: Comparison of post-fire GNDVI mean index value change over time……..34

Figure 8: Comparison of post-fire NBRI mean index value change over time……..35

Figure 9: ΔNBR profile for each fire event……36

Figure 10: Comparison of post-fire SATVI mean index value change over time……..37

Figure 11: Return to pre-fire conditions profile for six key indices after Carinda Rd fire (15/03/16 – 26/03/16)…….39

Figure 12: Return to pre-fire conditions profile for six key indices after Cresswell fire (25/02/15 – 14/03/15)…….40

Figure 13: Return to pre-fire conditions profile for six key indices after Masmans fire (29/12/14 – 06/01/15)…….40

Figure 14: Comparison of post-fire unsupervised classifications for the three fire events……42

Figure 15: Changed in burned pixel classification for Neural Networks classifier over time……...43

Figure 16: Changed in burned pixel classification for Random Forest classifier over time……..44

Figure 17: Changed in burned pixel classification for Support Vector Machine classifier over time…….46

Figure 18: Comparison of time taken for indices to return to pre-fire conditions across the three fire events……..47

List of Tables

Table 1: Table showing different bands of radar, their properties, and their common applications...7

Table 2: Properties of wildfire events analysed in study……...20

Table 3: List of spectral indices used in the study and how they were calculated. Adapted from Leutner & Horning (2017). s = Slope of the soil line, L = soil brightness factor (0.5)…….23

Table 4: Parameters for K-means/Iso-Cluster unsupervised classifier……..25

Table 5: Parameters for Random Forest Classifier……26

Table 6: Parameters for Neural Net Classifier……...26

Table 7: Parameters for Support Vector Machine Classifier…….27

Table 8: Highest (left) and lowest (right) index values Std. dIndex values in Masmans fire event..39

Table 9: Average commission and omission error rates for each classifier per fire event……31

Table 10: Categories of burn severity for the ΔNBR. Adapted from Escuin et al. (2008)....…….....35

Table 11: Time taken for each index to return to its mean pre-fire value by fire event…….....41

List of Equations

Equation 1: Calculation of dIndex (difference mean index value)…….28

Equation 2: Standardisation of dIndex value……..28

List of Appendices

Appendix 1: Accuracy results of Random Forest Classifiers…….58

Appendix 2: Commission and omission error rates of each classifier by fire event……..61

Appendix 3: Three-minute thesis poster submission for Wetlands in Drylands (WiDs) 2017 conference……..63

Appendix 4: WiDs 2017 conference abstract……64

Appendix 5: Index of sensors and their characteristics…….65

Acronyms and Definitions

Acronym	Definition
(A)NN	(Artificial) Neural Network
CTVI	Corrected Transformed Vegetation Index
DN	Digital Numbers
DVI	Difference Vegetation Index
ETM+	Enhanced Thematic Mapper Plus
EVI	Enhanced Vegetation Index
EVI2	Two-band Enhanced Vegetation Index
GEMI	Global Environmental Monitoring Index
GNDVI	Green Normalised Difference Vegetation Index
MNDWI	Modified Normalised Difference Water Index
MSAVI	Modified Soil Adjusted Vegetation Index
MSAVI2	Modified Soil Adjusted Vegetation Index 2
MSS	Multispectral Scanner
NBR/NBRI	Normalised Burn Ratio/Normalised Burn Ratio Index
NDVI	Normalised Differential Vegetation Index
NDWI	Normalised Difference Water Index
NDWI2	Normalised Difference Water Index 2
NIR	Near Infrared
NRVI	Normalised Ratio Vegetation Index
OLI	Operational Land Imager
RF	Random Forest
RVI	Ratio Vegetation Index
SAR	Synthetic Aperture Radar
SATVI	Soil Adjusted Total Vegetation Index
SAVI	Soil Adjusted Vegetation Index
SLAVI	Specific Leaf Area Vegetation Index
SR	Simple Ratio Vegetation Index
SVM	Support Vector Machine
SWIR (1/2/3)	Short-wave Infrared (Bands 1/2/3)
TIR/TIRS	Thermal Infrared/Thermal Infrared Sensor
TM	Thematic Mapper
TVI	Transformed Vegetation Index
TTVI	Thiam’s Transformed Vegetation Index
WDVI	Weighted Difference Vegetation Index

Acknowledgements

I would like to acknowledge the efforts and support of my research supervisors Hsing-Chung (Michael) Chang, Kerrie M. Tomkins, and Timothy J. Ralph, and recognise their instrumental role in the delivery of this thesis. I would also like to thank the Department of Environmental Sciences of the Faculty of Engineering, Macquarie University, for their general support as a candidate in the MRes program.

I would also like to thank the NSW Office of Environment and Heritage for their assistance with issues pertaining to legacy environmental data access, as well as their ongoing commitment to the Wetlands in Drylands research group. I would like to acknowledge the NSW National Parks and Wildlife Service for their role in this project and commend them for their active role in supporting research.

I would like to acknowledge the United States Geological Survey (USGS) for providing data from the Landsat missions free of charge to the community, without which this s would not have been possible. I would like to acknowledge the R core team for providing the R open source programming language free of charge to the community, without which this project would not have been possible.

Thesis Abstract

This thesis examines the accuracy and reliability of using conventional remote sensing methods in wetland environments, specifically for detecting and analysing burn scars and post-fire recovery. To date, the methods have been applied in dryland environments post-fire but have yet to be tested comprehensively elsewhere, particularly in large floodplain wetland environments that also experience regular wildfires. These ecosystems possess unique physical characteristics that may pose challenges to orthodox remote sensing techniques, such as different vegetation composition, soil moisture prevalence, and post-fire vegetation regrowth rate. This thesis also aims to provide a preliminary insight into how the current methods could be modified or further developed to achieve the high levels of accuracy gained in measuring burn scars in dryland environments. It was found that spectral indices that measure green vegetation cover, particularly the GNDVI, the EVI2, the NBRI, and the SATVI, are more suitable for detecting burn. It was also found that supervised classifiers, were more accurate than unsupervised classifiers at determining burned areas. From the results, it was concluded that, by a measure of the assessed metrics, post-fire wetland ecosystems typically regenerate to pre-fire conditions within a year of the fire event occurring. However, different conditions can significantly decrease the time taken for regeneration, with some indices returning to pre-fire values as early as 100 days post-fire.

1. Preface

1.1 Introduction and Relevance

Remote sensing has played a significant role in the history of natural hazards management, being used to analyse data of and inform management efforts for a range of natural disasters. One such natural disaster of interest is bushfires, which, due to their potentially catastrophic outcomes for human and natural environments, require analysis and assessment to limit or prevent the damage they cause where possible. As techniques for mapping the patterns and behaviours of fire have evolved over time, the utilisation of remote sensing technologies for fire detection has become more prevalent, as they allow for a unique approach to spatial data that is difficult to achieve through other methodologies (L. B. Lentile et al., 2006). Technological advancements in the fields of imagery, data management and computing have driven this increased relevance of remote sensing for fire history mapping, with these developments allowing for significant increases in spectral, spatial, and temporal resolution, as well as data processing at unprecedented scales and an unparalleled ease of access to publicly available data (L. B. Lentile et al., 2006).

Remote sensing techniques provide many advantages over in-field data collection, including faster and easier data collection processes, widely available historical data, and the ability to analyse large areas over much shorter time periods than traditional methods. While remote methods cannot be used as a complete replacement for scientific data analysis, they provide many unique insights that traditional field sampling measures cannot. In studies where the areas of analysis may span several square kilometres, traditional field-based measurement methods can be costly, time consuming, and also potentially limited in spatial coverage, as data are often collected only at certain points as opposed to across the entire study area. Therefore, remote sensing methods, with their many advantages and unique form of analysis, are a prime candidate to measure the spatial extent and severity of the burn scars left by bushfires.

The process of mapping burn scars allows researchers to determine the area affected by the fires and also their severity, the results of which are crucial information to preventative and rehabilitative efforts (Escuin, Navarro, & Fernández, 2008). Monitoring the temporal change of burn scars also provides a unique insight into the response of the ecosystem to the fire event, and how it regenerates back to its original conditions (Miller & Yool, 2002). There are myriad factors that affect the accuracy and efficacy of mapping burn scars, such as the spectral range and other capabilities of the sensor, the characteristics of the surveyed surface cover, and any potential atmospheric interference, such as from smoke, haze, or clouds (Goodwin, Collett, Denham, Flood, & Tindall, 2013). In wetland areas especially, there are some unique challenges that need to be considered, such as the

typically quick vegetation regrowth rate, the high probability for increased presence of moisture, and the diverse nature of vegetation characteristics within a small physical area (Klemas, 2011). Wetland ecosystems in dryland environments in Australia are often characterised by a few distinct vegetation types, including but not limited to reed/marsh, shrubland, sclerophyll forest, and open/cleared land, and because of their location within dryland environments, they are not perennially inundated. Wetlands often differ in their response to fire events when compared to dryland fires, which primarily arises from this different vegetation composition and density, and a tendency to have higher vegetation and soil moisture content when inundated (Kotze, 2013). If a wetland is completely inundated at the time of a fire event, there is a limit to the damage that can be caused, as the reed bed and the lower parts of the plants are submerged, shielding them from the intense heat and damaging impacts of the fire event. The results of this is an ecosystem that is partially damaged, but will likely regenerate quickly as the most vital parts of the plants have been left largely untouched (Kotze, 2013). Conversely, if the wetland is dry at the time of the fire event occurring, and the plants are burnt down to the reed bed, then the damage is far more significant as the plants have been mostly degraded or completely destroyed, and the ecosystem will take much longer to regenerate to pre-fire conditions. This variability of ecosystem composition and potentially rapid regeneration of wetland vegetation poses a challenge to conventional remote sensing methods that rely on information generated at infrequent intervals in the order of weeks to fortnights. Therefore, a combination of multi- and hyperspectral imagery, as well as active sensing methods like radar or light detection and ranging (LiDAR), are recommended to achieve a comprehensive analysis of the key variables of the study site (Kasischke, Melack, & Craig Dobson, 1997; Ozesmi & Bauer, 2002).

Thesis Aims and Structure

This thesis aims to:

1. Compare conventional remote sensing methodologies and their suitability for measuring burn scars in wetlands.
2. Understand the behaviour of ecosystem regeneration in post-fire wetland environments.
3. Provide information on fire extent and recovery that can be utilised for preventative and rehabilitative management efforts.

This thesis begins with a review of literature on remote sensing based land cover analysis. The main body of the research is presented in the style of a journal article which has been prepared for later submission. The thesis then concludes with a synthesis of the main findings, the significance of the research to the field, and suggestions for further work.

1.2 Previous Research on Remote Sensing Based Land Cover Analysis

1.2.1 Remote Sensing Methods and Techniques

A core component of remote sensing is satellite based imaging, which uses a variety of spectral bands to capture a diversity of information from the imaged areas at different wavelengths of electromagnetic radiation (EMR). They exist under two broad categorisations; active remote sensing systems, which propagate EMR towards an area to be sensed and then measure the signal response (e.g. radar, lidar), or passive remote sensing systems, which utilise EMR from external sources to sense an object or area (e.g. spectroradiometer, camera without flash) (Graham, 1999). There are a multitude of sensors aboard the numerous satellites that orbit the earth, which are sensitive to visible light, infrared, radio waves, microwaves, and other EMR. Many of these imaging techniques have been used to analyse wetland areas, for purposes such as vegetation mapping and classification, boundary and extent mapping, and ecological health evaluation (Klemas, 2011). This diversity of imagery technologies is accompanied by a diversity of advantages, disadvantages and outputs from each type. As such, it is common for different imaging sensors to be used in combination to utilise their individual strengths, as well as covering their shortcomings.

There are two distinct subtypes of optical remote sensing systems, namely multispectral sensors and hyperspectral sensors, based on the number of bands and their spectral widths. A multispectral sensor is one that is sensitive to multiple electromagnetic frequencies, and typically those outside of the visible light spectrum. The wavelengths covered by these sensors can include but are not limited to; visible, infrared variations, thermal, etc. Some common examples of these sensors include the multispectral scanner (MSS), thematic mapper (TM), enhanced thematic mapper (ETM+), and operational land imager/thermal infrared sensor (OLI/TIRS) aboard Landsat missions 4/5, 7, and 8 respectively. A multispectral sensor does not typically cover wavelengths in a directly continuous manner, rather leaving space between the wavelengths covered by the specified ‘bands’, e.g. Landsat 8 band 2 (Blue) – 0.41µm to 0.51µm, band 3 (Green) – 0.53µm to 0.59µm, and band 4 (Red) – 0.64µm to 0.67µm. This is in contrast to a hyperspectral sensor, which by definition covers continuous wavelength in visible, near infrared and shortwave infrared spectra. The Hyperion sensor aboard Earth Observer 1 (EO-1), for example, covers between 0.357µm and 2.576µm in 220 bands, allocating one band to each .01µm increase in wavelength (United States Geological Survey (USGS), 2011). Both multispectral and hyperspectral scanners can cover the same area of the electromagnetic spectrum, but it is the fineness of the resolution in which they cover them that defines their categorisation as multispectral or hyperspectral.

There is a significant and comprehensive selection of satellites, sensors, and spectral products available for the detection of large scale disturbances to vegetation cover caused by bushfires. The section below details some of the options that have been used to map burn scars previously.

Passive Remote Sensing Sensors

Landsat Missions

The Landsat program of satellites and sensors is the longest serving in history, beginning in July 1972 with Landsat 1. For this study, the relevant satellites include Landsat 4/5 TM, Landsat 7 ETM+, and Landsat 8 OLI/TIRS, as these have coverage over the last two decades. Landsat 4/5 consisted of two essentially identical satellites, both of which carried thematic mappers (TM) and multispectral scanners (MSS) covering seven spectral bands from 0.45-12.50µm across both scanners. Covered bands include visible RGB, NIR, TIR, and MIR, which can be used to make band false colour band composites like the example shown in Figure 1 below.

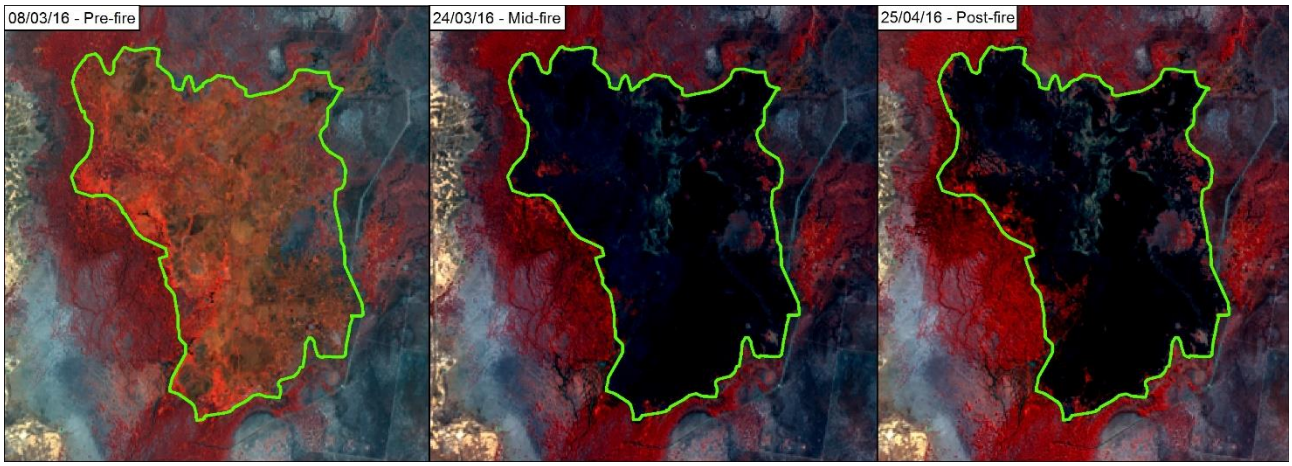

Figure 1: False colour infrared view of Macquarie Marshes wetland with fire boundary overlay before and after a fire. (Landsat 8 OLI/TIRS – Blue, Green, and Near-infrared band composite.)

The satellite followed a near-polar, sun-synchronous orbit with a 16-day repeat interval, and a 185km swath width with resolutions of 30m (bands 1-5, 7), and 120m (band 6). Landsat 7 is the next generation of the satellite program, and as such carries the new Enhanced Thematic Mapper Plus (ETM+), which covers eight spectral bands from 0.45-12.50µm. Covered bands are almost identical to Landsat 5, with the addition of the panchromatic band 8, which is imaged at a spatial resolution of 15m. Orbital characteristics remain the same as Landsat 4/5. The newest addition to the Landsat program is Landsat 8 OLI/TIRS, which began in February 2013, and is comprised of two sensors: and operational land imager (OLI) and thermal infrared sensor (TIRS). These newer generation sensors allow Landsat 8 to capture additional spectral bands, its range of capture now measuring from 0.43-12.51µm. The new bands include coastal aerosol (band 1), cirrus (band 9), and two TIR bands (bands 10-11). A detailed index of each sensors bands and characteristics is available in Appendix 6. Spatial resolutions remain largely the same as previous iterations of the

program, with the exception of the TIR bands, which have a resolution of 100m. Orbital characteristics are again the same as the previous Landsat satellites. Landsat is perhaps the most commonly utilised space-borne imaging system when performing vegetation analysis, which is largely due to its high spatial and temporal resolution, spectral coverage, and ease of availability. Landsat imagery has been used in vegetation extent and burn scar mapping, and is typically employed as the imagery component for NDVI/NBR operations and classification processes (Escuin et al., 2008; Viedma, Meliá, Segarra, & Garcia-Haro, 1997). Additionally, Landsat has already been used in previous studies focusing on the mapping of burned areas in wetlands to relative success by utilising the thermal infrared band of the ETM+ module aboard Landsat 7 (Cassidy, 2007). Landsat data is readily available dating back decades, of good spatial, temporal, and spectral resolution, and versatile for classification purposes, making it an excellent candidate for inclusion in this research study.

MODIS

Moderate Resolution Imaging Spectroradiometer (MODIS) is a wideband sensor duo also on-board the NASA EOS Terra and Aqua satellites, and began its mission in December 1999. MODIS covers 36 spectral bands from 0.62-14.385µm, which covers from the visible range through to the middle infrared range (MIR). The sensors cover the earth in a sun-synchronous, low-earth, near-polar orbit, with a temporal resolution of one to two days. Swath width is 2300km, and spatial resolutions vary by band, and are as follows: 250m (bands1-2), 500m (bands 3-7), 1000m (bands 8-36). A detailed index of each sensors bands and characteristics is available in Appendix 6. While the spatial resolution of these sensors are relatively coarse, the temporal resolution is far higher than typical imaging products, allowing the MODIS system to provide unique benefits to mapping burn scars in areas of quick vegetation regeneration (Ling, Du, Zhang, Li, & Xiao, 2015; Loboda, Hoy, Giglio, & Kasischke, 2011). While MODIS has quite a coarse spatial resolution, the temporal and spectral resolution combined with the long archive of data and history in burn scar mapping makes it a good candidate for inclusion in this research project.

Sentinel-2A/B

The Sentinel-2A/B satellite system began in 2015 with the launch of Sentinel-2A on the 23/06/15, which was followed by the launch of Sentinel-2B almost two years later on the 7/03/17. The two satellites run in tandem in a sun-synchronous orbit, resulting in a repeat interval of five days. The satellites house multispectral instruments covering twelve spectral bands from 0.443-2.19µm, which covers the visible wavelengths through to the shortwave infrared (SWIR) wavelengths. Swath width is 290km. and spatial resolution is 60m for bands 1, 9 & 10, 10m for bands 2-4 & 8, and 20m for bands 5-7, 8A, 11 & 12. A detailed index of each sensors bands and characteristics is available in

Appendix 6. Due to its higher spatial, spectral, and temporal resolution, Sentinel-2 fills many criteria for accurate burn scar mapping (Delegido, Verrelst, Alonso, & Moreno, 2011). However, as it only recently became operational and only one satellite was in orbit for a part of the time period analysed, it is not suitable for this study.

Active Remote Sensing Methods

Radar is another form of electromagnetic radiation based sensing than can be used to measure, detect and analyse numerous surface characteristics (such as the ecological and geomorphological) as well as atmospheric characteristics, and is available in both space-borne and airborne applications (Kasischke et al., 1997). In the context of burned area mapping, radar-based imaging processes can be used to examine various characteristics of the surface of the Earth, which can then be used to create indices of burned areas. These can include the properties of vegetation (height, density, and extent etc.), soil moisture, or surface roughness, amongst others (Dubois, Zyl, & Engman, 1995; Durden, Zyl, & Zebker, 1989). These different and diverse physiognomies of the surface can pose a challenge to remote sensing systems, as their inherent diversity can require different methodologies to acquire accurate results.

Synthetic aperture radar (SAR) is a form of microwave imaging technology that operates across multiple wavelengths, and is capable of reading both linear and circular polarisations (Bourgeau-Chavez, Kasischke, Brunzell, Mudd, & Tukman, 2002). A current radar satellite mission, the European Space Agency (ESA) Sentinel 1A/B, has imaging sensor, with swath widths from 80km to 400km, and spatial resolutions from 5m x 5m to 25m x 100m (European Space Agency (ESA), 2017). Radar images are also largely unimpeded by diverse atmospheric conditions, such as cloud cover or rain, providing a distinct advantage over satellite based visible/infrared spectrum imagers such as the Landsat array (Bourgeau-Chavez et al., 2002). Over the many years since the authors conducted their initial study, imaging and computing technology has drastically improved, with contemporary radar sensors alone allowing for far finer spatial resolutions through ultra-wideband and terahertz SAR instruments.

SAR can be used to measure fire scarring in dryland areas, which is achieved by measuring physical changes in a post-fire environment as a means of generating indices to inform the mapping of fire affected areas. An article by Bourgeau-Chavez et al. (2002) explored the use of C-band SAR for fire scar mapping in boreal forest environments. By using electromagnetic radiation (EMR) on the microwave end of the frequency spectrum, the authors were able to measure a distinct scattering and interference caused by the excess moisture prevalent in post-fire soil, which was used as an indicator of a recent fire event (Bourgeau-Chavez et al., 2002). Radar imaging techniques can also be utilised to directly map vegetation coverage and density, which is useful to analyse the

characteristics of recently burned areas and map them accordingly (Bourgeau-Chavez et al., 2002; Ling et al., 2015; Stroppiana et al., 2015).

There are a few inherent characteristics of radar that make it suitable for a diversity of imaging applications. For example, the different wavelengths that comprise radar imaging methodologies can be used to measure and analyse different vegetation indices (canopy cover and depth, vegetation extent and density, etc.), through the level of backscatter, reflection and penetration they achieve. Current radar imaging services include both the airborne and space-borne varieties, and use ranging and detection methods across wavelengths ranging from larger than 1m (Frequency - 300MHz) down to 2.5cm (Frequency - 12GHz). A summary of the different bands used, their properties, and their applications is present in the table below.

Table 1: Table showing different bands of radar, their properties, and their common applications.

	Frequency Range	Wavelength Range	Uses
P-band	<300MHz	>1m	Canopy penetration mapping
L-band	1-2GHz	15-30cm	Moisture backscatter analysis
S-band	2-4GHz	7.5-15cm	Soil moisture analysis
C-band	4-8GHz	3.75-7.5cm	Vegetation fuel load analysis
X-band	8-12GHz	2.5-3.75cm	High resolution imagery

Wavelength

P-band

P-band radar uses electromagnetic waves in the >1m wavelength/sub-300MHz frequency range, which is within the very high frequency range (VHF). Electromagnetic waves at this frequency have wavelengths in the one to ten metre range and can be used for general applications such as broadcasting and communications. In imaging technologies, P-band radar can be used to measure characteristics of multi-layered vegetation such as forests, as it's long wavelength combined with the correct polarisation allows it to penetrate through dense canopies, and achieve secondary returns of up to 10-15m from lower layers of vegetation (Hensley et al., 2001; Rignot, Zimmermann, & Zyl, 1995).

L-band

L-band radar uses electromagnetic waves in the 15-30cm wavelength/1-2GHz frequency range, which is within the ultra-high frequency range (UHF). Electromagnetic waves at this frequency have wavelengths in the 15-30cm range and can be used for general applications such as communications and device networking. The most common use of L-band radar in surface imaging is using backscatter analysis to detect soil moisture or vegetation density, and subsequently infer/estimate biomass (Lucas et al., 2010; Mitchard et al., 2009, 2011). An article by Paloscia,

Macelloni, Pampaloni, & Sigismondi (1999) determines that both P- and L-band radar wavelengths are useful for detecting forests and herbaceous vegetation respectively, when analysed using HV polarisation methods.

S-band

S-band radar uses electromagnetic waves in the 7.5-15cm wavelength/2-4GHz frequency range, which is within the ultra-high frequency (UHF) and super-high frequency (SHF) ranges. Electromagnetic waves at this frequency have wavelengths in the 7.5-15cm range, and are conventionally used for wireless networking, and short-range inter-device communications. S-band is not as commonly used for vegetation analysis as the other bands mentioned, but can be combined with L-band to perform soil moisture analysis on post-fire areas (Bolten, Lakshmi, & Njoku, 2003).

C-band

C-band radar uses electromagnetic waves in the 3.75-7.5cm wavelength/4-8GHz frequency range, which is within the super-high frequency range (SHF). Electromagnetic waves at this frequency have wavelengths in the 3.75-7.5cm range and are conventionally used for short-range communications or weather forecasting radars. C-band radar has applications in fuel load estimations for forest ecosystems, where it is typically combined with P-band and L-band to determine indicators of fuel loading, such as canopy density and foliage moisture content (Saatchi, Halligan, Despain, & Crabtree, 2007).

X-band

X-band radar uses electromagnetic waves in the 2.5-3.75cm wavelength/8-12GHz frequency range, which is within the super-high frequency range (SHF). Electromagnetic waves at this frequency have wavelengths in the 2.5-3.75cm range, and common uses include terrestrial and outer-space communications, and civilian, military, and government radar. X-band radar imaging can either be airborne or space-borne, and allows for much higher resolution imagery than the previously mentioned bands. Previous articles on the applications of X-band SAR have found that it is effective at detecting vegetation and biomass, but can also be useful for mapping the distribution of wetlands in a dryland environment when combined with a cooperative C-band system (Stofan et al., 1995).

It is evident that certain wavelengths are better suited for specific applications, and each have their own unique limitations in terms of resolution, penetration depth, and sensitivity. As such, a common approach for surveying an area with significant surface diversity and variation is to utilise multiple radar imaging bands to combine their individual strengths in a multi-frequency approach (Evans, Farr, Ford, Thompson, & Werner, 1986). This approach is typically complimented with the

use of multiple divergent polarisations, each of which are sensitive to different surface characteristics, to achieve a more comprehensive analysis of the target area (Mougin et al., 1999).

Polarization

Another key characteristic of electromagnetic radiation that can influence the data output of radar-based remote sensing system is the polarisation of the outgoing electromagnetic waves. In regards to radar systems, electromagnetic waves can be polarised in two ways, including linear polarisation and circular polarisation (Collett, 2005). Linear polarisation is considered as 'single direction', and consists primarily of two 'planes' of polarisation; the horizontal (side to side movement) and the vertical (up and down movement) (Collett, 2005). The polarisation of the electromagnetic wave is determined by the arrangement of the electric and magnetic fields generated by the sensing apparatus, which are always at angles perpendicular to each other. The polarisation of the electric field component is the used to describe the overall polarisation of the electromagnetic wave. Knowing the desired polarisation of the electromagnetic wave will then dictate the mounting arrangement of the sensor or antenna itself, in order to receive the correct result. Using this physical property of electromagnetic radiation, it is possible to use known and measured polarisations as data to construct images, a process known as polarimetry (Collett, 2005). In the context of remote sensing for environmental and geomorphological surveying, differing polarisations can be used to gain diverse data from different surface types. Polarisations of different alignments can be used to sense a wide variety of surfaces, from grassed areas, to forest canopies, to urban areas, each of which respond differently to different polarisations (Treuhaft & Cloude, 1999).

1.2.2 Spectral Indices and Transformations

A spectral index (or vegetation index) is an equation typically performed on different bands of multispectral sensors to develop a metric that is a direct representation of a certain physical characteristic of the area sensed. Numerous indices have been developed over the past 50 or so years to serve a number of purposes, such as detecting biomass density, surface water, soil brightness, and burn scars, amongst others (Silleos, Alexandridis, Gitas, & Perakis, 2006). Often, spectral indices can prove suitable to detect changes or disturbances that they were not designed to, as events like fires tend to cause a significant change in the spectral signature of the ground. The following section details some spectral indices that have been commonly utilised for the detection of burn scars in post-fire environments. There are various indices which can be used for the detection of burn scars, such as the leaf area index (LAI), the burned area index (BAI), and composite burn index (CBI), are not discussed here because while they are still pertinent to the topic, they were not utilised in the study for various reasons.

Simple Ratio (SR)

The simple ratio vegetation index (SR) was one of the first spectral indices to be developed, and was published by Birth & McVey in 1968. It is generated by the simple equation NIR/Red, and was used to test the different spectral reflectance properties of turf types and life stages, as the NIR band was largely reflected by the structure of green vegetation (Birth & McVey, 1968). The SR has primarily been found to be a good indicator of vegetation cover and leaf area, but has also been used to detect burn scars, such as in a study by Boer et al. (2008) where it was included in a regression model to determine **Δ**LAI as an indicator of burned areas. In this study, it was found the SR was more sensitive to changes in LAI than the NDVI, and the results produced were comparable in accuracy to those generated by using **Δ**NBR to assess the area (Boer et al., 2008). However, due to its somewhat simplistic nature, it has some inherent errors, such as the potential for zero value denominators and a lack of scale linearity (Silleos et al., 2006).

Normalised Differential Vegetation Index (NDVI)

Perhaps the most commonly used method for detecting the severity and extent of past fires is the Normalised Difference Vegetation Index (NDVI), which utilises multispectral imagery to perform a change detection operation on vegetated surfaces by subtracting the red band from the NIR band and dividing it by the sum of the red and NIR bands, resulting in an accessible -1 to 1 representation scale (Silleos et al., 2006). The significance of the red and NIR bands especially is that healthy green vegetation will reflect a majority of the radiance in this part of the spectrum, allowing for the easy delineation of vegetated and non-vegetated areas, as well as vegetation health, quality and density (Knipling, 1970). While an NDVI is perhaps the most common approach for vegetation change detection, it is not without its deficiencies, and is susceptible to skewed results due to atmospheric interference (Pereira, 1999). Additionally, newer indices that can take advantage of the higher spectral diversity in contemporary satellites are showing results with finer discriminations within burned areas, resulting in a more detailed and comprehensive analysis (Chuvieco, Martín, & Palacios, 2002).

Normalised Burn Ratio Index (NBR/NBRI)

The NBR is another commonly employed burn index, operating similarly to the NDVI, but substituting the visible red band for the shortwave infrared band because of the distinct patterning of burned areas that can be measured by infrared radiation (Kontoes, Poilvé, Florsch, Keramitsoglou, & Paralikidis, 2009). Studies by Escuin et al. (2008) determined that the NBR modulations was generally more accurate than the NDVI at mapping pre-/post-fire displacements, making it particularly apt for measuring fire severity. However, the accuracy of the NBR is strongly dependent on the type of vegetation being analysed, and previous research by Mallinis & Koutsias

(2012) concluded that the NBR produced relatively variable results depending on survey area, with a result of 95.04% matching to the control group fire extent for one study, and as low as 90.06% in another. Areas with greater uniformity of surface covering typically result in a more accurate analysis when using the NBR (Kontoes et al., 2009). See Figure 1 below for a visual comparison of the NBR and NDVI processes.

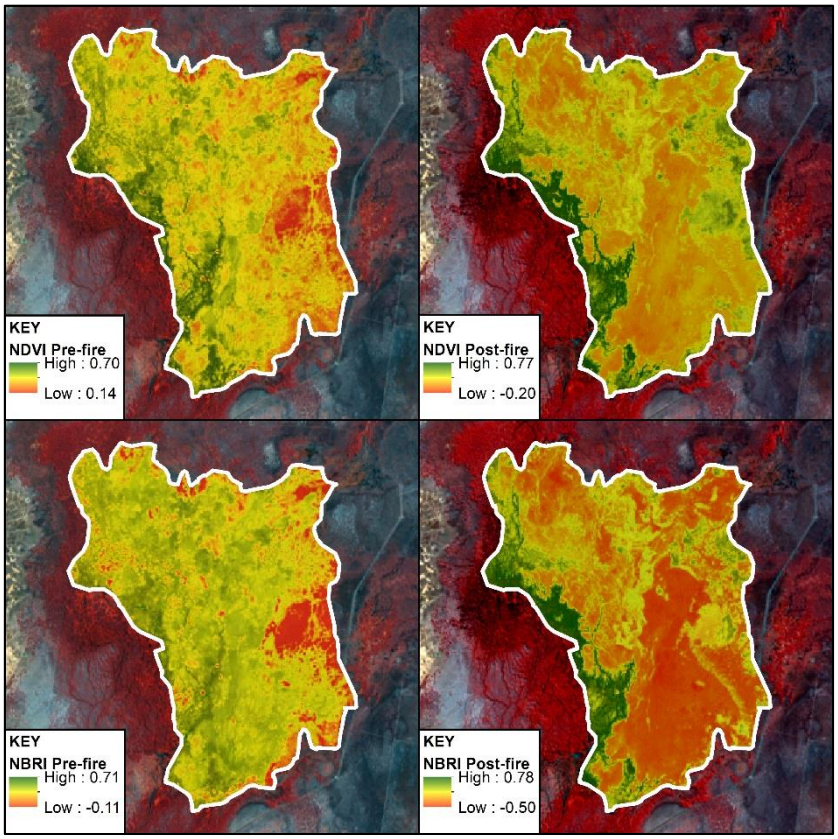

Figure 2: Comparison between NDVI (top) and NBRI (bottom) pre-fire (left – taken 8/03/16) and post-fire (right – taken 24/03/16), generated from Landsat 8 OLI/TIRS imagery. (Background:

Normalised Difference Water Index (NDWI)/Normalised Difference Water Index II (NDWI2)

The NDWI/NDWI2 are different to the indices mentioned above in that they are designed to measure open water features and vegetation liquid water respectively, as opposed to vegetation cover or other variables. The NDWI is calculated by subtracting the NIR band from the green band and dividing it by the sum of the green and NIR bands, and the NDWI2 is calculated by subtracting the SWIR2 band from the NIR band, and dividing it by the sum of the NIR and SWIR2 bands (Gao, 1996; McFeeters, 1996). Further research by Xu (2006) led to a modification of the NDWI by substituting the NIR band for the SWIR2 band, which further highlighted open water features, while simultaneously supressed noise from built-up land, vegetation, and soil. These indices have been used in the detection of fire previously, but generally in a supportive capacity, such as in a study by Ding, Zhang, Fan, & Chen (2012), in which the MNDWI was used to mask out areas of open water, before being combined with a number of other indices like the NBR, BAI, SAVI, and GEMI to be

used as training data for a support vector machine classifier. However, the effect of the significant amounts of moisture and open water bodies present in wetland ecosystems has on the ability of these indices to measure the direct disturbances to vegetation caused by fires is not well documented, and may well confuse these moisture based indices.

Tasseled Cap Transformation

Indices are not the only method of transforming imagery into simplified products ready for analysis. The Tasseled Cap Transformation technique is a different type of method for manipulating the raw spectral data of multispectral sensors (i.e. thematic mappers) into a format that allows for the extraction of physical scene characteristics from the spectral data (Crist & Cicone, 1984). By transforming the spectra into a usable orientation, the Tasseled Cap is able to derive three key components of the area surveyed: brightness – a measure of the total reflectance or soil brightness of the scene, derived by calculating a weighted sum of all the bands of the image, greenness – an indicator of healthy green vegetation cover, measured as the contrast between NIR and visible bands, and wetness – a measure of soil moisture, calculated by contrasting the sum of the NIR and visible bands with the sum of the long-IR bands (Crist & Cicone, 1984). These three surface characteristics can be used as determinants of land cover change from a number of causes, including flooding, deforestation, or bushfires, and can also be used as supplemental or supporting information in other surface cover classification methods (Dymond, Mladenoff, & Radeloff, 2002; Jin & Sader, 2005).

When used alone, the Tasseled Cap method can be used as the Tasseled Cap Index (TCI), which provides an absolute measure of the three components (brightness, greenness, and wetness) normalised across a scale of -1 to +1 (Haywood, Verbesselt, & Baker, 2016). This index can be calculated for sequence of imagery before and after a known event, and the relative differences in the components compared to create a profile of surface characteristics over time. The TCI has been used in previous research to map disturbance dynamics in the wet sclerophyll forests of the Central Highlands of NSW, Australia, where it was tested with the normal burn ratio (NBR) to determine the accuracy of delineating between acute and low severity surface cover change events and their respective agents (Haywood et al., 2016). The combination of the TCI and NBR fitted to random forest classification methods was found to be ~ 72% accurate at distinguishing between acute and low severity disturbance events, and up to ~ 95% accurate at determining the agent responsible for the disturbance (Haywood et al., 2016). This suggests that that the use of the TCI, in conjunction with other suitable indices, is appropriate for the delineation of burn scars in post-fire environments.

1.2.3 Classification Methods

Imagery classification is a process that categorises input spectral data based on a predetermined set of algorithms into distinct spectral classes, and can be performed in multiple unsupervised (no external training data) or supervised (external training data required) forms (Lu & Weng, 2007). The use of classifications to determine burned areas is well researched, with numerous previous studies comparing and contrasting the merits and deficiencies of diverse classification techniques for detecting burn scars (Brumby et al., 2002; Chen, Moriya, Sakai, Koyama, & Cao, 2016; Mallinis & Koutsias, 2012; Patterson & Yool, 1998; George P. Petropoulos, Vadrevu, Xanthopoulos, Karantounias, & Scholze, 2010). Research by Mallinis & Koutsias (2012) critically evaluated ten different classification approaches for burn scars in post-fire environments, determining the overall accuracy and confidence interval for each method. However, the study ultimately concluded that different approaches are suitable for different subject areas, and it is still not completely understood which approach is suitable for each area (Mallinis & Koutsias, 2012). Discussed below are some of the more common methodologies for classifying burned areas from imagery with varying levels of accuracy and efficiency.

Random Forest (RF)

The RF classification is a supervised, machine-learning ensemble method consisting of a 'forest' of individual decision trees, utilising the mode of the input classes as the output result (Breiman, 2001). Previous research has established the random forest method as an accurate classifier of land cover types, which could indicate that it would be an effective approach to extracting burn scars from otherwise relatively spectrally homogenous environments (Gislason, Benediktsson, & Sveinsson, 2004, 2006). Land cover classification results with accuracies over 90% have been recorded, and the method generally requires less user input and training, and computer resources to achieve similarly precise results as other supervised classification methods (Pal, 2005; Rodriguez-Galiano, Ghimire, Rogan, Chica-Olmo, & Rigol-Sanchez, 2012). However, due to the relative 'youth' of the random forest classification methodology when compared to ANN and SVM, not much research has been undertaken to determine the effectiveness of this method when applied to burn scar mapping, but the practice is of course similar to land cover classification.

Support Vector Machine (SVM)

SVMs are supervised machine learning models that use learning algorithms for classification and regression analyses on datasets. In the context of classifying burn scars in vegetation, SVMs operate in a linear fashion, using class borderline pixels to establish more defined boundaries between classes (Mallinis & Koutsias, 2012). On average, SVM was the most accurate across the three study sites in the Mallinis & Koutsias (2012) article, with an overall accuracy of 91.11%. Two articles by

(George P. Petropoulos, Kontoes, & Keramitsoglou, 2011) and Petropoulos, Knorr, Scholze, Boschetti, & Karantounias (2010) confirm the accuracy of this method with comparable studies in similar areas, achieving results with accuracies of 95.87% and 94.6%, respectively. SVMs have been used on varied multispectral imagery, such as those captured by ASTER, MODIS, SPOT and Landsat satellites, with similar success, and can prove to be a cost effective and accurate method of classifying burn scars in post-fire environments (Mallinis & Koutsias, 2012; G. P. Petropoulos et al., 2010). However, as these studies were all conducted in areas of limited surface covering diversity within the Mediterranean, the aptness of this classifier may be limited in alternate ecosystems like wetlands.

Neural Networks (NNs)

Neural networks (NN) or artificial neural networks (ANN) are a supervised classification method consisting of a collection of individual yet interconnected neurons or nodes designed to mimic the operation of the human brain by providing a systematic approach to problem solving and pattern identification (Civco, 1993). In a comparison between an ANN and a Spectral Angle Mapper (SAM) conducted by Petropoulos, Vadrevu, Xanthopoulos, Karantounias, & Scholze (2010), it was found that ANNs are typically a highly precise methodology for classifying burnt areas in Landsat TM imagery, with an overall accuracy of 90.29% and mean absolute percentage difference from the designated control data of ~1%. Similarly accurate results were also obtained consistently across the three study sites in the Mallinis & Koutsias (2012) article, returning accuracy values of 96.49%, 94.21%, and 95.05%. These results render it one of the most accurate methods of burn scar classification as tested by Mallinis & Koutsias (2012), and its versatility across these study sites may be indicative of its aptitude for classifying burn scars in wetland areas.

Logistic Regression (LOG)

Logistic regression is a form of statistical analysis predicated upon the relationships of numerous independent variables to a dichotomous dependent variable, which in this case is a burned or unburned pixel (Mallinis & Koutsias, 2012; Pu & Gong, 2004). In the Mallinis & Koutsias (2012), LOG is the third most accurate classification method overall, while also retaining a relatively high confidence interval. A study conducted by Pu & Gong (2004) on single L7 ETM+ images in the forests of California also concluded that the LOG methodology was highly accurate, and typically on par with the results generated by the neural network approach. However, LOG managed to achieve those results in a much shorter timeframe, rendering it a more efficient method to use, especially if time is considered a factor (Pu & Gong, 2004).

Classification and Regression Trees (CARTs)

A CART analysis consists of the application of either a classification tree or regression tree to a dataset when the output is predicted to be qualitative or quantitative, respectively. These techniques can then be used to construct more complex statistical analysis methods, such as a random forest approach, which can be employed to achieve a faster classification rate by using multiple trees in tandem. When used in the Mallinis & Koutsias (2012) study, CART analysis had varying results across the three sample sites, with higher accuracy in the Kassandra study area, which is a generally semi-arid ecosystem comprised largely of pine stands and shrubs. This type of environment is of course very different to the intended study area for this research project, so classification accuracy through this method may vary with the physical characteristics of the environment.

Spectral Mixture Analysis (SMA)

Linear or least squares SMA operates on the assumption that the input spectrum is a "linear combination of the end-member spectra weighted by the percentage ground cover of each end-member of all components within the pixel" (Mallinis & Koutsias, 2012). An end-member is described as being a pure version of the spectra that corresponds to a given land cover class, and can be generated from the image or from reference material (Mallinis & Koutsias, 2012; Maselli, 2001). Previous research by Elmore, Mustard, Manning, & Lobell (2000) and Small (2001) have found SMA to be an effective classification tool for vegetation in diverse surface types, often exceeding the accuracy of the NDVI by up to 20%. In the Mallinis & Koutsias (2012) study, SMA had varying results depending on the survey area, but was typically less accurate in comparison to the other techniques. These sites, however, all consist mostly of dense forest, woodland, or shrubland, which may react differently to classification techniques compared to wetlands (Mallinis & Koutsias, 2012). Additionally, SMA results had on average lower confidence indices, suggesting that SMA is perhaps one of the less accurate methods of classification.

There has been a significant research effort into analysing the capability of diverse remote sensing techniques for the detection and mapping of burn scars in multiple types of dryland environments, however the research for whether the same techniques are applicable in wetland ecosystems is lacking, and even more so for wetland ecosystems that are not perennially moist. As such, this study aims to provide a preliminary insight into the suitability and efficacy of these remote sensing techniques, and the nature of ecosystem regeneration in post-fire environments.

2. Journal Paper

A Comparative Analysis of Remote Sensing Techniques for Burn Scar Mapping in the Macquarie Marshes, Australia

2.1 Abstract

This study explores the impact of bushfire events in the Macquarie Marshes with three key objectives: (1) to compare remote sensing methodologies and their ability to measure burn scars in wetland areas; (2) to understand the behaviour of ecosystem regeneration in post-fire wetland environment; and (3) to provide information on fire extent and recovery that can be utilised for preventative and rehabilitative management efforts. Focusing on three fires that occurred between 2014 and 2016, the methodology employs a multi-part approach. Part one included generating a range of spectral indices on satellite imagery collected pre- and post-fire and comparing the relative responses of each index to the fire event. Part two includes the comparison of four classification methods, including neural networks (NNs), support vector machine (SVM), random forest (RF) and K-means/Iso-Cluster on the imagery pre- and post-fire. Finally, an extended term analysis was performed to observe ecosystem regeneration in post-fire wetland environments. The indices found to be most efficient at determining burned areas were those designed to measure burned areas or areas of green vegetation, such as the normalised burn ratio index (NBRI), or the green normalised difference vegetation index (GNDVI). The SVM classifier proved to be the most adept at identifying burned pixels, with an average error rate of 36.02%, with the RF and NN classifiers close behind at 42.13% and 43.69% respectively.

2.2 Introduction

Bushfires are known to be one of the more devastating natural disasters that affect Australia, often resulting in significant and widespread environmental and socioeconomic damage that can take years to decades to recover from (Stephenson, Handmer, & Betts, 2013). They cause the destruction of natural and human environments, and disrupt and unbalance normal ecosystem functioning for extended periods of time (Stephenson et al., 2013). That is not to say that bushfires are not without their benefits, as it is true that many Australian flora species rely upon the intense energy of bushfire events for germination and to stimulate new growth in post-fire environments (Gill et al., 1999). For wetland environments, bushfires can be catastrophically damaging if the vegetation is burnt down to the reed bed, resulting in a lengthy regeneration period that may permanently change the characteristics of the landscape (Kotze, 2013).

However, the extent of the impacts of bushfires on wetland environments are not always clear, and previous fire events that have occurred in wetland environments have caused varying amounts of environmental and socioeconomic damage, usually depending on the state of inundation at the time (Kotze, 2013). Conversely, assuming the wetland has a sufficient level of inundation, a bushfire event can act as a stimulant for new growth, and areas that have been burned can regenerate within the space of weeks or months, as can be seen in Figure 3 below (Aber, Pavri, & Aber, 2012). This is often faster than the return time of many satellites, which is typically captured on a minimum 16-day cycle. As such, detecting burn scars left by fires in wetland areas can pose issues when the same methodologies that are used in drylands are applied without the consideration of the quick regeneration, unique vegetation, and variable moisture composition present in wetlands in drylands.

Figure 3: Wetland environment at one week post-fire (Left) and the same area at three weeks post-fire (Right). Image credit Peter Berney, Office of Environment and Heritage (OEH), NSW.

There exist many methods for assessing the characteristics and distribution of land cover change with multispectral satellite imagery, with two of the most common being spectral indices and classifications. Previous research in this field has focused on the analysis of two major components of a fire event: spatial footprint/area burnt, and severity/intensity, and while these two components are frequently related in a given fire event, measurement and detection methodologies can be distinctly different (Mallinis & Koutsias, 2012; Rogan & Franklin, 2001). This study compares 22 different spectral indices and four classification methods to determine the efficacy of each in identifying and quantifying the extent and severity of burn scars in comparison to a control dataset.

With consideration to the current knowledge in the field, this study is designed to provide insight into existing knowledge gaps by fulfilling a selection of key aims. Firstly, through a process of comparison by statistical analysis, this study aims to determine the most suitable method for delineating burn scars in wetland environments, with regard to accuracy, but also efficiency and

applicability for practical implementations. Secondly, this study aims to analyse the response of wetland ecosystems by monitoring the post-fire regeneration of three fire events in the Macquarie Marshes. Thirdly, this study aims to translate what is learnt from the first two aims into practical information that could be used to inform management efforts in post-fire environments, so that the environmental and socioeconomic impact of bushfire events in wetland areas can be limited where possible.

2.3 Methods

2.3.1 Site Selection

This study will focus on fires that occurred in the Macquarie Marshes, a large inland wetland system covering 19,850 ha located in the centre-north of New South Wales (NSW), Australia (See Figure 4 below). The area also contains two of Australia's 65 Ramsar listed wetlands; the Macquarie Marshes Nature Reserve (northern and southern sections, ARSN 28), and U-block. This designation indicates that this area is of high environmental significance, and plays a key role as a component of the surrounding environment, providing habitat for numerous threatened ecological communities, and performing vital ecosystem services (Department of the Environment and Energy, 2009).

The study area is a wetland ecosystem situated within a dryland environment, which lends it some unique physiological characteristics in terms of biota, hydrology, and geomorphology. It can be separated into two major areas, the Southern Marshes, which is generally accepted as the area south of Gibson Way, and the Northern Marshes, which is the area north of Gibson Way, and the area of interest for this study (See Appendix 1). The Marshes contains a mixture of landscapes and vegetation types, but the most dominant cover types are chenopod shrublands, grasslands, sclerophyll forests and open plains, which cover close to 73,000 of the total 243,918 ha of the Marshes. Bodies of open water and partially submerged vegetation are also common depending on seasonality, which are in stark contrast to dryland environments that are commonly proliferated by woodland ecosystems or dry grassy shrubs, and, especially in inland Australia, can be characterised by protracted periods of low moisture (Power, Casey, Folland, Colman, & Mehta, 1999).

The Macquarie Marshes was chosen as the study area for several reasons; the wetlands are significant in size, they have a diversity of vegetation types, and they are currently the focus of a dedicated research group for wetlands in drylands. The size of the wetlands also allows for larger fires to occur, which in turn leave larger burn scars upon the earth, which results in their easier detection through remote methods and higher resolution analyses.

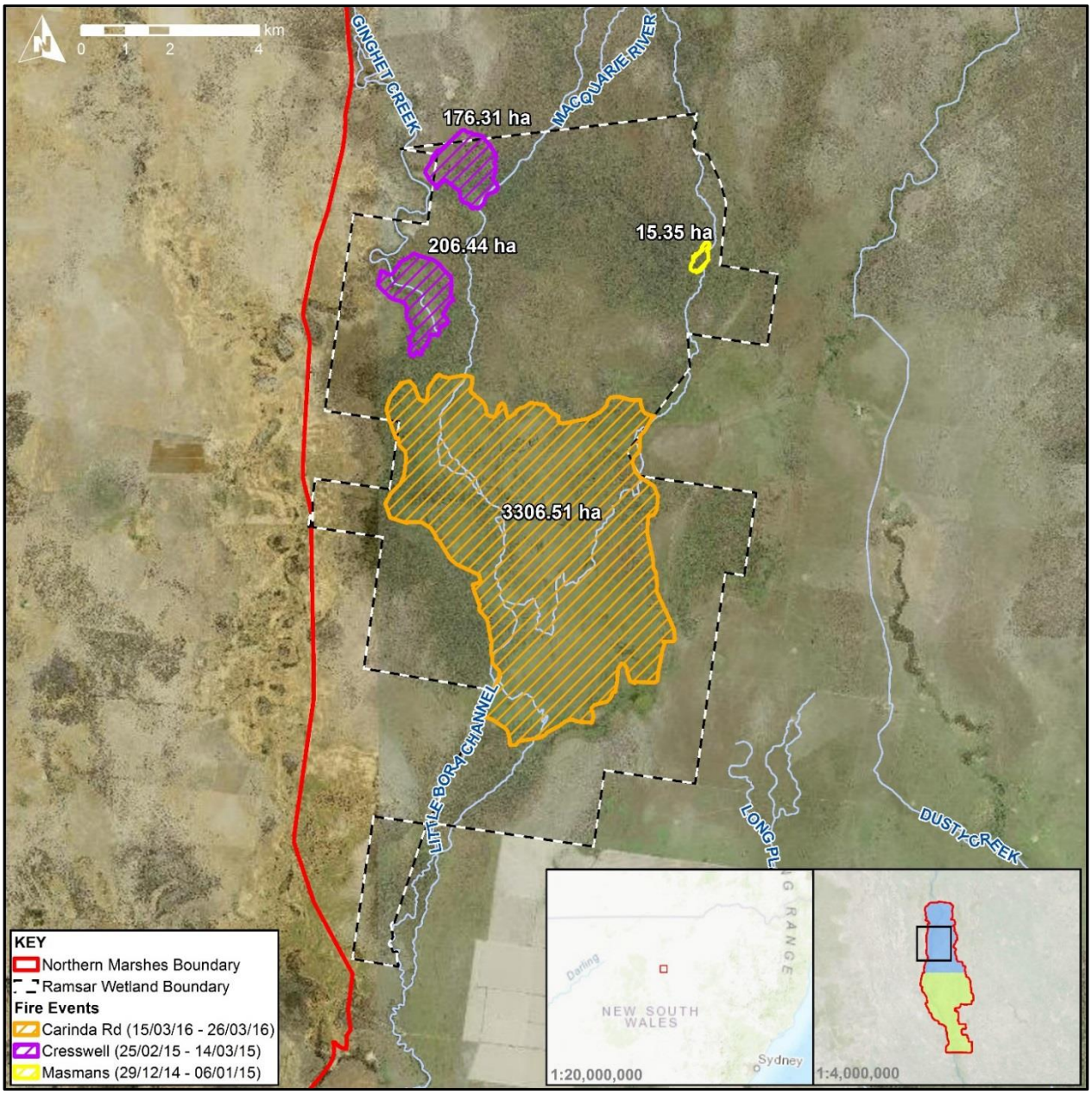

Figure 4: Map of study area and fire events. Imagery © Land and Property Information (LPI), 2015.

There is a well-documented short-term history of fire in this area, supported by both empirical and anecdotal evidence. Datasets indicate that several bushfire events of natural and anthropogenic origin, have occurred in past decade, resulting in a varied pool of samples which will contribute towards more robust results. Additionally, these fire events were also reported to be of significant extent and intensity, making them easier to analyse due to their larger spatial footprint in relation to satellite resolution. A summary of the bushfire events analysed in this study can be found in the Table 2 below.

Table 2: Properties of wildfire events analysed in study.

Fire Name	Start Date	End Date	Duration	Area (Ha)	Perimeter (KM)
Carinda Rd Fire	15/03/16	26/03/16	11 days	3308.9	30.8
Cresswell Fire	25/02/15	14/03/15	17 days	383.0	12.3
Masmans Fire	29/12/14	6/01/15	8 days	15.4	1.9

2.3.1 Data Acquisition

As the temporal period being used for analysis is not insignificant in size and the size of the study area crosses multiple image footprints, a more refined method for fire identification and spatial positioning is required, so a chronology of imagery for the study area can be formed. The best approach was determined to be a collation of several different methods so as to achieve the most accurate and comprehensive identification of fire occurrences in the study area.

NSW OEH/NPWS Datasets

The New South Wales Office of Environment and Heritage (OEH) and National Parks and Wildlife Service (NPWS) are two leading environmental management organisations in Australia, and each create and maintain datasets relating to vegetation and bushfires. The OEH has supplied a native vegetation community extent map and historical bushfire extent map of the Macquarie Marshes in for this project. The vegetation community dataset consists of polygon features used to show the extent of different types of vegetation, and also contains attribute data for the polygons, such as vegetation characteristics and scientific names (See Figure 5 below). The historical fire dataset contains polygon features delineating the maximum spatial footprint of the fire event, and relevant attribute data pertaining to the events, such as date, duration, and origin, amongst others. This dataset will be used as the primary method of fire event identification.

Sentinel Hotspot

Geoscience Australia's Sentinel Hotspot system was then used to verify the fire events recorded in the NPWS dataset. The Sentinel system uses data from three sensors (Advanced Very High Resolution Radiometer [AVHRR], Moderate Resolution Imaging Spectroradiometer [MODIS], and Visible Infrared Imaging Spectroradiometer [VIIRS]) to establish a hotspot dataset representing active fires over the last 72 hours. Active fire points were then cross-referenced with the NPWS fire history records, verifying the occurrence of the selected fire events mentioned previously.

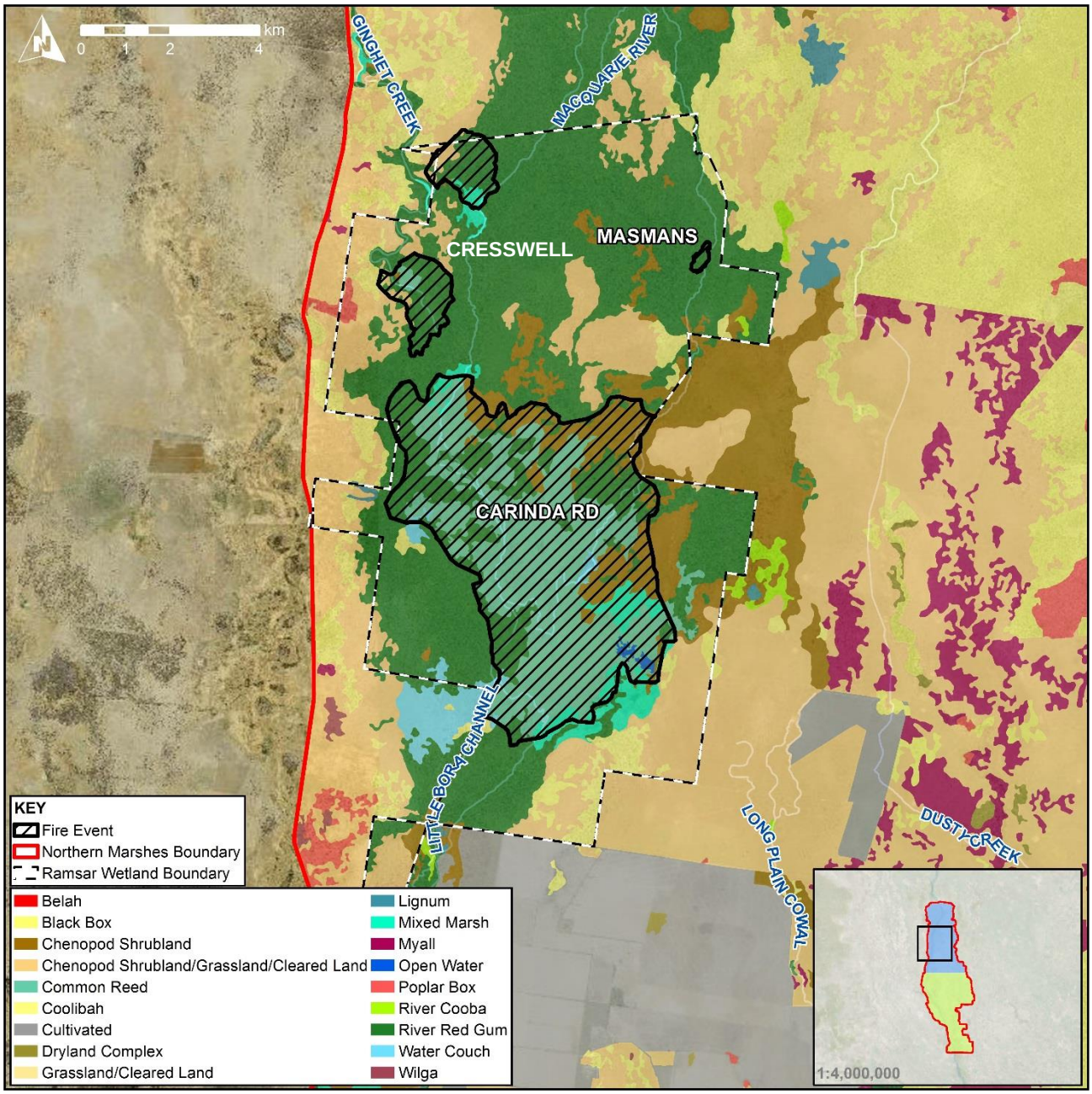

Figure 5: Map of vegetation communities for study area. Data from OEH (2013). Imagery © Land and Property information (LPI), 2015.

Satellite Imagery

Once the spatial and temporal locations of the fires were identified and confirmed, suitable imagery data were obtained. Imagery from the Landsat program was selected for its reasonably high spatial resolution and moderate return time of 16 days, properties which have resulted in it being commonly utilised for burn scar mapping in previous research (Leigh B. Lentile et al., 2006). Additionally, the increased spectral resolution in the infrared segment of the electromagnetic spectrum compared to typical tri-band or quad-band imagery can also be used to generate spectral indices such as the NDVI and NBR amongst many others, which utilise the infrared frequencies to

monitor vegetation and provide more accurate burn scar detection (Holden, Smith, Morgan, Rollins, & Gessler, 2005).

By cross referencing the fire dates from the NPWS dataset and the image intervals of the Landsat satellites, it was possible to identify that all fires had adequate imagery coverage before and after the event. Imagery was then acquired from the Operational Land Imager/Thermal Infrared Sensor (OLI/TIRS) of the Landsat 8 mission at intervals around the fire events, with one image being chosen as close as possible before the fire, and then multiple images at intervals during and after the fire event. Images were then also acquired at repeat intervals during and after the fire event, where available. Images were collected for dates amounting to one or two months' worth post-fire, as it was assumed that the typically quick regeneration time of wetland vegetation species (reliant upon inundation) would obscure any scars past this time (Cassidy, 2007). Table 3 below shows the details of the imagery acquired for each fire event.

2.3.2 Data Pre-processing and Quality Control

Radiometric Corrections

While the imagery used for analysis was already processed to USGS Level 1-C standards (including georectification and projection to WGS 1984 UTM Zone 55N), further radiometric corrections were recommended by many of the classification methods, including the conversion to radiance or reflectance for some indices. Radiometric correction was implemented with the radCor function of the RSToolbox package in the R statistical programming language, which applies corrections and converts the digital numbers to radiance values (Leutner & Horning, 2017). Cloud masking was also applied where appropriate using the cloudMask function of the RSToolbox R package. Cloud masked pixels were marked as 'no data', and not included in any analysis or result calculations.

2.3.3 Data Analysis

The two forms of imagery analysis selected for this project are spectral indices and imagery classifications. These two techniques utilise the same input data, can provide distinctly different results, and each have their own unique strengths and weaknesses. Spectral indices are typically simpler than imagery classifications, and generally consist of simple band arithmetic from a few bands of a raster image but can also include known constants or parameters in some cases. Imagery classifications are characteristically more complex and can require additional user input that isn't necessary with the calculation of spectral indices. However, imagery classifications can be generated using all the available bands of the raster image, allowing them to better define spectrally unique areas, which ultimately results in a more accurately classified image.

Spectral Indices

Multiple spectral indices are chosen for this project, with the intent to compare the outputs of the indices and determine the accuracy and efficacy of each method. The indices in Table 4 below were calculated in R for each image using the spectralIndices function of the RSToolbox package (Leutner & Horning, 2017). Spectral indices were then calculated on each individual image and compiled in chronological order to form a time sequence analysis, so any changes over time could be observed at the pixel level (Yang & Lo, 2002). This sequencing process allows for the observation and analysis of post-fire vegetation regrowth, and any associated behaviours or patterns it may display.

Table 3: List of spectral indices used in the study and how they were calculated. Adapted from Leutner & Horning (2017). s = Slope of the soil line, L = soil brightness factor (0.5).

Index	***Name***	***Source***	***Bands***	***Formula***
CTVI	Corrected Transformed Vegetation Index	Perry, 1984	red, NIR	*(NDVI + 0.5)/sqrt(abs(NDVI + 0.5))*
DVI	Difference Vegetation Index	Richardson, 1977	red, NIR	*s * NIR - red*
EVI	Enhanced Vegetation Index	Huete, 1999	red, NIR, blue	*2.5 * ((NIR - red)/(NIR + C1 * red - C2 * blue + L_evi))*
EVI2	Two-band Enhanced Vegetation Index	Jiang, 2008	red, NIR	*2.5 * (NIR - red)/(NIR + 2.4 * red + 1)*
GEMI	Global Environmental Monitoring Index	Pinty, 1992	red, NIR	*(((NIR^2 - red^2) * 2 + (NIR * 1.5) + (red * 0.5))/(NIR + red + 0.5)) * (1 - ((((NIR^2 - red^2) * 2 + (NIR * 1.5) + (red * 0.5))/(NIR + red + 0.5)) * 0.25)) - ((red - 0.125)/(1 - red))*
GNDVI	Green Normalised Difference Vegetation Index	Gitelson, 1998	green, NIR	*(NIR - green)/(NIR + green)*
MNDWI	Modified Normalised Difference Water Index	Xu, 2006	green, SWIR2	*(green - SWIR2)/(green + SWIR2)*
MSAVI	Modified Soil Adjusted Vegetation Index	Qi, 1994	red, NIR	*NIR + 0.5 - (0.5 * sqrt((2 * NIR + 1)^2 - 8 * (NIR - (2 * red))))*
MSAVI2	Modified Soil Adjusted Vegetation Index 2	Qi, 1994	red, NIR	*(2 * (NIR + 1) - sqrt((2 * NIR + 1)^2 - 8 * (NIR - red)))/2*
NBRI	Normalised Burn Ratio Index	Garcia, 1991	NIR, SWIR3	*(NIR - SWIR3)/(NIR + SWIR3)*
NDVI	Normalised Difference Vegetation Index	Rouse, 1974	red, NIR	*(NIR - red)/(NIR + red)*

NDWI	Normalised Difference Water Index	McFeeters, 1996	green, NIR	*(green - NIR)/(green + NIR)*
NDWI2	Normalised Difference Water Index	Gao, 1996	NIR, NIR2	*(NIR - NIR2)/(NIR + NIR2)*
NRVI	Normalised Ratio Vegetation Index	Baret, 1991	red, NIR	*(red/NIR - 1)/(red/NIR + 1)*
RVI	Ratio Vegetation Index	N/A	red, NIR	*red/NIR*
SATVI	Soil Adjusted Total Vegetation Index	Marsett, 2006	red, SWIR2, SWIR3	*(SWIR2 - red)/(SWIR2 + red + L) * (1 + L) - (SWIR3/2)*
SAVI	Soil Adjusted Vegetation Index	Huete, 1988	red, NIR	*(NIR - red) * (1 + L)/(NIR + red + L)*
SLAVI	Specific Leaf Area Vegetation Index	Lymburner, 2000	red, NIR, SWIR2	*NIR/(red + SWIR2)*
SR	Simple Ratio Vegetation Index	Birth, 1968	red, NIR	*NIR/red*
TVI	Transformed Vegetation Index	Deering, 1975	red, NIR	*sqrt((NIR - red)/(NIR + red) + 0.5)*
TTVI	Thiam's Transformed Vegetation Index	Thiam, 1998	red, NIR	*sqrt(abs((NIR - red)/(NIR + red) + 0.5))*
WDVI	Weighted Difference Vegetation Index	Richardson, 1977	red, NIR	*NIR - s * red*

Classifications

The process of image classification categorises pixels into new distinct classes based upon a particular training process or algorithm. Two major types of machine learning classification exist: supervised classification and unsupervised classification. Supervised classifications require the input of external training data in the form of sample data with ‘known’ values, which for the classification process to apply to a broader scale (Kotsiantis, 2007). Unsupervised classifications use no known data from external sources, and learn solely within the target dataset (Kotsiantis, 2007). This study will compare four classification techniques against each other, and evaluate their effectiveness, efficiency, and accuracy in discerning spectral class differentiations from imagery in the study areas. All of the classifications were performed on a ten band raster stack of Landsat 8 bands, generated by the stackMeta function of the RSToolbox package in the R programming suite. This stack included all of the available 30m resolution bands including the downsampled thermal infrared bands but excluded the 15m panchromatic band and quality assessment band.

Training Polygons

The three supervised classification methods used in this study require training and/or validation data to train the classifier. These data were created in the form of spatial vector data delineating the target spectral classes in the imagery. Training polygons were created for the set of imagery for each fire event as opposed to every image, as it was determined that this would provide the best compromise between time taken for the analysis and accuracy of results. Polygons were created as equally as possible in size, shape and amount for each class, and to further ensure training equality, a random sample of 100 pixels was taken from within the designated areas to use as the final training data. This process was repeated to create a second set of training data that was used as a validation dataset, and it was ensured that the training and validation sets were spatially exclusive, so as not to introduce potential training errors. Areas inside the NPWS fire boundary were selected as the 'Burned' class, and the rest were distributed amongst the majority land cover types included in the scene, including rivers/open water bodies, wetland marsh, dryland vegetation, field/paddock, etc. A cross validation accuracy analysis and confusion matrix was created for the training polygons of each fire event and is available in Appendix 1.

Unsupervised Classification (K-Means/Iso-Cluster)

Both of these classifiers were completed using the RSToolbox package of the R programming suite. The unsupervised classification was undertaken using the K-means/Iso-Cluster method in the unsuperClass tool of the RSToolbox package in the R programming suite. Eight classes were chosen as a recommended default for general heterogenous vegetation unsupervised classification as per Horning, Leutner, & Wegmann (2016), and the number of starts and samples were linked to that. Normalisation was used to align all values to the same scale for better comparison. Table 5 below details the parameters used for the classification.

Table 4: Parameters for K-means/Iso-Cluster unsupervised classifier.

Parameter	Value
Classes	8
Starts	50
Samples	10000
Normalisation	Yes

Random Forest (RF)

The random forest classifiers were performed using the superClass and predict tool of the RSToolbox and randomForest packages in R respectively. The classifier was first trained using the previously mentioned training polygons, and a classification model was developed. This was then fitted to the entire image, and cross-validated by a secondary 'validation' training polygon set to

achieve a more accurate result. A summary of the parameters used for the RF classifier can be observed in Table 5 below.

Table 5: Parameters for Random Forest Classifier.

Parameter	Value
Sampling	Random
Sampling Points	100
Cross Validation	True
N/A Values	Omitted

Neural Networks (NN) and Support Vector Machine (SVMs)

The neural network and support vector machine classifications were performed using the Neural Net Classifier and Support Vector Machine tool in ENVI 5.3. Training data for the classifications was prepared via the method mentioned above, but the polygons were split into their respective classes in ArcMap to be consumed properly by ENVI. For the neural net classifier, the training threshold contribution was set to 0.9 as more complete footprints were desired over absolute pixel accuracy. 1000 training iterations was considered to typically be a good balance between achieving the 0.1 training RMS exit criteria and taking sufficient time to process. The training rate was set on the low end, as a more accurate classification was desired over a faster classification process. For the SVM classifier, the radial basis function kernel type was chosen as it is generally known to work well in most cases. The penalty parameter was set relatively high to avoid excessive smoothing, and the pyramid levels and classification probability threshold were kept low to increase the resolution of the classification and improve accuracy. Parameters for the tools are outlined in Tables 6 and 7 below.

Table 6: Parameters for Neural Net Classifier.

Parameter	Value
Activation	Logistic
Training Threshold Contribution	0.9
Training Rate	0.2
Training Momentum	0.9
Training RMS Exit Criteria	0.1
Number of Hidden Layers	1
Number of Training Iterations	1000

Table 7: Parameters for Support Vector Machine Classifier.

Parameter	Value
Kernel Type	Radial Basis Function
Gamma in Kernel Function	0.1
Penalty Parameter	100
Pyramid Levels	0
Classification Probability Threshold	0

2.3.4 Validation of Results

Once the outputs have been generated, they will need to be validated to determine their accuracy and robustness. Due to the remoteness of the study site and the time at which the fire events occurred, there is no sample data available for conventional ground truthing means. As such, the main source of validation is therefore the OEH/NPWS fire boundary dataset, as all results are being compared to the spatial footprints contained within this and the results then compared against one another. This dataset was created through empirically robust means, which included the burn perimeter being flown and tracked with GPS data daily and supplemented with digitisation from high resolution aerial imagery where needed. It provides a suitable control against which the other techniques in this study can be assessed. However, further research efforts would ideally validate the results of this study against suitable first-hand, empirical ground control data.

The supervised classifiers underwent an internal validation process as part of the classification process. The random forest supervised classifier is unique amongst the methods used in that it utilises a secondary set of external data for validation. This is achieved by utilising a set of validation polygons, which are essentially the same as the training polygons except they must differ in spatial location, to confirm that the training of the random forest model is accurate and valid. Validation accuracy is provided in the form of Kappa values, confidence intervals, and P-values, and confusion matrices.

2.4 Results and Analysis

2.4.1 Results of Spectral Indices

The change in spectral indices from pre- to post-fire environments varied widely between fire events, but a majority of the indices calculated exhibited a significant response to the fire occurring when compared to the background change during the same period. The ability of an index to detect a fire event was determined by the differential between the mean index value from within the fire boundary of the pre-fire image and the first mid-fire image as per the equation below, and is expressed as dIndex (e.g. dNDVI, dEVI2) (Escuin et al., 2008; Miller & Thode, 2007).

$$dIndex = abs(Mean\ Index\ Value_{pre-fire} - Mean\ Index\ Value_{mid-fire})$$

Equation 1: Calculation of dIndex (difference mean index value).

As not all of the indices shared a similar scale (e.g. -1 to 1), they were then standardised across the recorded range of mean values for the extended profile (~ 1 year) to show the relative change of the mean index values, which allowed for a direct comparison of all indices. The values were standardised as per the following equation:

$$Standardised\ (Std.)\ dIndex = \frac{dIndex}{abs(Mean\ Index\ Value_{max} - Mean\ Index\ Value_{\min})}$$

Equation 2: Standardisation of dIndex value.

Carinda Rd Fire

The Carinda Rd fire event displayed the greatest disturbance to land cover change as viewed through the profile, with a high majority of the indices exhibiting a strong positive or negative swing away from pre-fire conditions in the post-fire result. The indices that exhibited the most significant change between pre- and post-fire environments were the EVI2, the RVI, the NBRI, the NDWI, and the GNDVI. Of the five indices that exhibited the most significant change between pre- and post-fire ecosystems, three utilise only the red and NIR bands, and two utilise the green and NIR bands. The changes observed in these indices over the pre-/post-fire period indicates a large decrease in the reflection of these bands after the fire event has occurred, indicating a significant loss of vegetation and the presence of a new surface covering which does not reflect these bands to the same degree. The indices that displayed the least degree of change between the pre- and post-fire environments of the Carinda Rd fire tended to have low dIndex values as well as low Std. dIndex values, with the exception of the SR, which showed a dIndex of 1.405, but had a total range of ~6, resulting in a low Std. Index value. Table 8 below displays the five highest and lowest values for the data series.

Cresswell Fire

The Cresswell fire exhibited lower average dIndex values than the Carinda Rd fire event, indicating that the total change in land cover between pre- and post-fire events in the Cresswell event was to a lesser degree than the Carinda Rd event. However, the Cresswell event does present on average higher Std. dIndex values, which would suggest that the Cresswell event was more impactful on its locality in the context of the profile. The indices that exhibited the most significant change between the pre- and post-fire environments of the Cresswell fire were the EVI2, the SATVI, the NBRI, the GNDVI, and the NDWI, which are largely similar to the most responsive indices for the Carinda Rd event, with the exception of the SATVI. Table 8 below displays the five highest and lowest values for the data series.

Masmans Fire

The average dIndex value for the Masmans fire event is lower again than the Cresswell event, suggesting that the Masmans fire had less of an on the spectral signature of the ground cover than the other two fire events. Additionally, the most responsive indices also changed somewhat, with the EVI2 and NBRI being replaced by the GEMI and SAVI as those with the highest dIndex values. Table 8 below displays the five highest and lowest values for the data series.

Table 8: Highest (left) and lowest (right) index values Std. dIndex values in Masmans fire event.

Carinda Rd					
Highest	**dIndex**	**Std. dIndex**	**Lowest**	**dIndex**	**Std. dIndex**
EVI2	0.601	0.891	**DVI**	0.138	0.403
RVI	0.446	0.643	**MNDWI**	0.15	0.37
NBRI	0.533	0.64	**MSAVI**	0.166	0.322
NDWI	0.368	0.632	**SLAVI**	0.371	0.275
GNDVI	0.368	0.632	**SR**	1.405	0.228
Cresswell					
Highest	**dIndex**	**Std. dIndex**	**Lowest**	**dIndex**	**Std. dIndex**
EVI2	0.316	0.905	**DVI**	0.094	0.528
SATVI	0.096	0.852	**MSAVI**	0.121	0.466
NBRI	0.293	0.744	**NDWI2**	0.105	0.353
GNDVI	0.204	0.693	**SR**	1.009	0.347
NDWI	0.204	0.693	**SLAVI**	0.216	0.344
Masmans					
Highest	**dIndex**	**Std. dIndex**	**Lowest**	**dIndex**	**Std. dIndex**
GNDVI	0.104	0.949	**EVI2**	0.129	0.46
NDWI	0.104	0.949	**MSAVI**	0.037	0.452
SATVI	0.079	0.913	**SR**	0.271	0.419
GEMI	0.079	0.878	**SLAVI**	0.027	0.198
SAVI	0.066	0.867	**NDWI2**	0.007	0.052

2.4.2 Results of Classifications

Unsupervised Classification

K-means/Iso-Cluster

The K-means/Iso-Cluster unsupervised classification proved to be the least discerning of the selection of classification methods used, with very little class variation within diverse vegetation communities, and little to no measurable detection of the disturbance caused by the fire across any of the events analysed. Class diversity, an indicator of spectral variation expressed as the number of unique classes that were classified within the fire boundary, averaged at three classes across the post-fire imagery for the Carinda Rd fire event, two classes for the Cresswell fire event, and two classes for the Masmans fire event. The areas in which the fires occurred were predominantly miscategorised in the same class as the surrounding unburned wetland marsh vegetation, shrub/grassland, or open watercourses. As the results were not meaningful, they are not shown here.

Supervised Classifications

Supervised classification accuracy was analysed with two metrics: (1) Commission error rate as % (false positive): the percent of total pixels classified as burned that were located outside of the NPWS fire boundary and shouldn't have been (2) Omission error rate as % (false negative): the percent of pixels within the NPWS fire boundary that were not classified as burned.

Neural Networks

The Neural Networks classifier was the least consistent performer of the supervised classifications, as its accuracy varied quite dramatically across the fire events, even so far as not detecting any burned pixels in the Masmans fire event imagery. The results of the Neural Net classifier are displayed in Table 9 below. As mentioned previously, the neural networks classification of the Masmans fire event failed to detect any burned pixels in any of the post-fire imagery, and instead frequently misclassified the area as the equivalent of either wetland marsh, low shrubland/grassland or sclerophyll forest.

Random Forest

The results of the random forest classifier varied across the different fire events, but generally showed a consistency of progression within the same fire event. The areas delineated as burned in the post-fire images were the smallest compared to the other two classifiers and tended to be scattered with pixels of other classes. The results of the random forest classifier can be found in Table 9 below, and the results of the cross-validation accuracy report can be found in Appendix 1.

Support Vector Machine

Despite being generally inefficient in terms of classifier training time, the SVM classifier produced some accurate results across the fire events, especially regarding the delineation of burned pixels. Other classes were also relatively accurately classified. The results of the analysis can be found in Tables 9 below.

Table 9: Average commission and omission error rates for each classifier per fire event.

Neural Net	**Commission Error Rate (%)**	**Omission Error Rate (%)**
Carinda Rd	13.97%	35.43%
Cresswell	34.99%	90.37%
Masmans	0.00%	0.00%
Average	16.32%	41.93%
Random Forest	**Commission Error Rate (%)**	**Omission Error Rate (%)**
Carinda Rd	0.06%	64.26%
Cresswell	0.36%	69.49%
Masmans	98.79%	33.95%
Average	33.07%	55.90%
Support Vector Machine	**Commission Error Rate (%)**	**Omission Error Rate (%)**
Carinda Rd	3.33%	34.81%
Cresswell	2.68%	63.65%
Masmans	93.91%	26.74%
Average	33.31%	41.73%

2.4.3 Detection of Burned Areas based on Spectral Indices

The results of the spectral indices analysis were quite varied, both between different fire events, and between the indices measured within a single event, but certain indices displayed consistently stronger responses to the fire disturbances than others. Of the spectral indices utilised, the most consistently effective and responsive indices were those that were targeted at measuring either the presence of burned areas, green vegetation cover, or soil moisture. This was achieved by utilising the green, red, near-infrared, mid-infrared, and thermal infrared bands of the satellites sensors, and occasionally some known constants, to analyse the reflected radiation of these wavelengths by the ground coverings in the scene and determine when a change in reflection occurs. Indices such as the green normalised difference vegetation index (GNDVI), the normalised difference water index (NDWI), the soil-adjusted transformed vegetation index (SATVI), the normalised burn ratio index (NBRI), and the enhanced two-band vegetation index (EVI2) showed very pronounced and significant responses to fire events, exhibited through a drastic change in values between the pre-fire image and the image taken immediately post-fire. Others, however, displayed far more subtle reactions to the fire events, with much smaller variations between pre- and post-fire environments.

Poorly performing indices were generally consistent across the separate fire events, and tended not to share similar properties or formulas, often using similar band combinations as indices that performed well, but to somewhat different results. A majority of the most poorly performing indices, such as the SR, the DVI, the MSAVI, the SLAVI, and the MNDWI, still elicited a response to the fire events, but in the context of the change measured across the rest of the profile and across the background, these responses were not as significant as the others. Poor performance can be the result of a number of variables, which most likely are caused by the not being designed for use with wetland vegetation and the potentially excessive presence of moisture when compared to dryland ecosystems (Chuvieco et al., 2002).

As one of the primary objectives of this paper was to gain an insight into the behaviour of vegetation regrowth in post-fire wetland environments, it is important to not only determine which remote sensing method can most clearly and accurately delineate the burn scars, but what the results of the methods tell us about what's happening on the ground to create this change. For example, within the range of the spectral indices used in the analysis, some focus on vegetation cover, some on the presence of moisture, and others on soil brightness or a lack thereof. Drilling down further upon that, these indices measure the response of the ground to certain wavelengths of electromagnetic radiation, which can reveal a significant amount of information about the surface of the study area.

EVI2

The EVI2 is similar to the NDVI in that it is a measure of vegetation cover, but the formula for calculating vegetation cover is different. Where the NDVI uses a simple ratio of the red and near-infrared bands, the EVI2 uses some known constants to better discern between vegetation and other ground cover types, such as soil and water, while simultaneously controlling for other variables like soil and atmospheric influences (Jiang, Huete, Didan, & Miura, 2008). The EVI2 showed a consistently significant response to the disturbance caused by all three fire events, which is observable as a large dip in the mid-fire and first post-fire images of the spectral index profile.

In the Carinda Rd fire event, the EVI2's most divergent value was the mid-fire image, which experienced a drop of approximately 0.62 from the pre-fire value. This indicates that a significant loss of green vegetation cover occurred between these two sampling points, a result that is consistent with the effects of a large bushfire. Following this large decrease, the profile displayed an accelerating increase for about three months, regaining 76% of its difference to the pre-fire value, before it experienced a small dip at roughly four months post-fire, as can be observed in Figure 6 below. The cause of this sudden yet small decrease is not clear, but is most likely attributable to external factors, as the profile began to increase again for the following three months, where it

reached a peak 0.08 above the pre-fire value at 0.84. The shape of this profile indicates that a level of green vegetation cover equivalent to that of the pre-fire ecosystem was present at ~ 208 days post-fire, with regrowth continuing to occur past this point. Similar results were observed in the

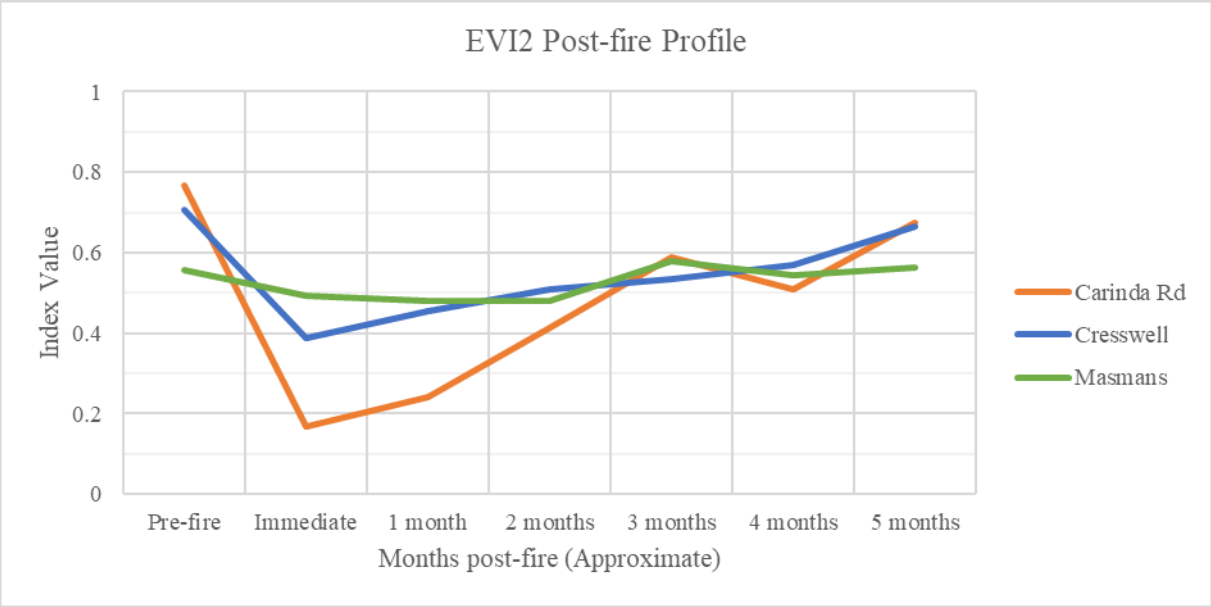

Figure 6: Comparison of post-fire EVI2 mean index value change over time.

Cresswell event, where the mid-fire image was the lowest value, and the most significant decrease throughout the profile at 0.31. The remainder of the Cresswell fire profile was characterised by an almost linear increase over the following seven months, a small dip that lasted for a month, and finally a return to the pre-fire value at 248 days. The response to the Masmans fire event was a little more subdued, but exhibited the same rough shape, albeit with a quicker return to the pre-fire level at 107 days, and a greater variability towards the tail-end of the profile.

GNDVI/NDWI

The green normalised difference vegetation index (GNDVI) and normalised difference water index (NDWI) utilise an inverse arrangement of the green and near-infrared bands to sense either the presence of green vegetation or water in the surveyed area, and as such are inextricably linked in their response to disturbances in the environment. Previous studies by Navarro et al. (2017) and Fernandez-Manso, Quintano, & Roberts (2016) have found the GNDVI to be an effective tool to detect and quantify burn scars, especially in areas of denser vegetation canopy cover that may otherwise confuse other indices such as the NDVI and NBR.

Like many of the other vegetation-based indices, the GNDVI displays a strong response to the fire event, dropping by 0.367 between the pre-fire and mid-fire images in the Carinda Rd fire event, by 0.204 in the Cresswell event, and by 0.092 in the Masmans event. The Carinda Rd and Creswell post-fire regeneration periods are both characterised with a steady increase over the subsequent

months, with minor dips and plateaus before returning to pre-fire conditions at 176 and 216 days respectively. Shortly after the point at which pre-fire values are reached, both profiles also exhibit a secondary plateau and decrease, which is likely unrelated to the impacts of the fire event.

The Masmans fire event shows a less aggressive post-fire regeneration, and after an initial significant increase in the secondary post-fire image, exhibits a plateau for the ensuing four months. The GNDVI eventually returns to pre-fire conditions at 251 days post-fire, but due to the surrounding variability, it is unsure whether this is the direct result of post-fire regeneration, or natural variability. Figure 7 below displays the post-fire profile of the GNDVI graphically.

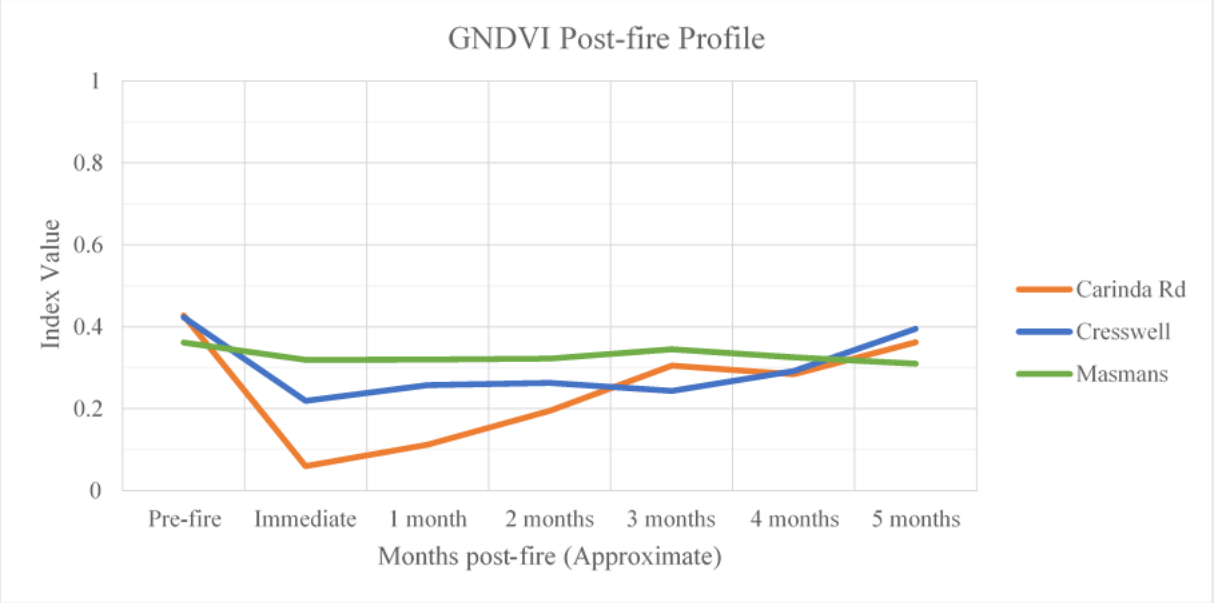

Figure 7: Comparison of post-fire GNDVI mean index value change over time.

NBRI / ΔNBR

The NBRI works similarly to the NDVI in that it is a simple ratio, but it substitutes the red band for one of the shortwave infrared bands, which is more sensitive to the vegetation loss caused by fire disturbance events. While the NBRI was designed for use in dryland systems, with a consideration of the phenological and compositional differences present in different environments, it is possible to apply the same technique to wetland ecosystems. The NBRI responded quite significantly to the large disturbances caused by the fire events in this study, displaying an almost absolute loss of infrared reflection in post-fire ecosystems. This was observable in the Carinda Rd fire event as a decrease from pre-fire to mid-fire value of 0.53, and as decreases of 0.29 and 0.16 in the Cresswell and Masmans fire events respectively. Like the other indices, the NBRI profile for the Carinda Rd fire shows strong increases almost immediately after the fire occurs, indicating that post-fire regrowth is prevalent across the area. A return to pre-fire values is seen at approximately 128 days post-fire, one of the fastest return times of the indices measured. The Cresswell fire profile exhibits different post-fire behaviour, characterised by an inconsistent but gradual rise in NBRI, with a

return to pre-fire values recorded at 216 days post-fire, suggesting that the regrowth for the Cresswell fire is not as strong as the Carinda Rd fire, despite it being a smaller, less severe event. These results are displayed graphically in Figure 8 below.

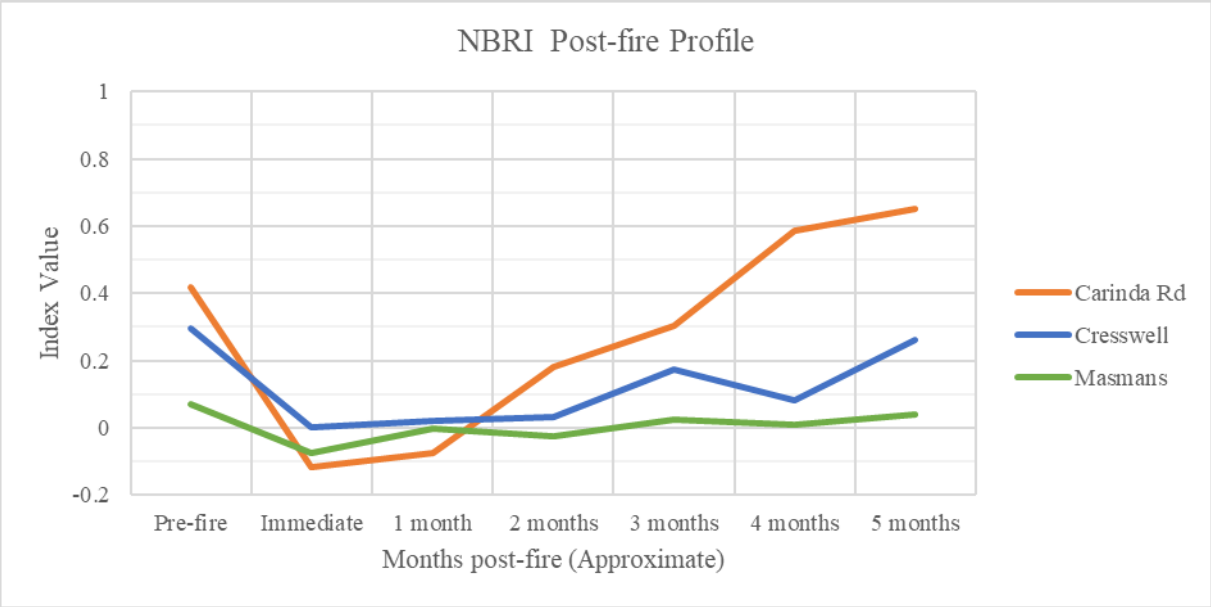

Figure 8: Comparison of post-fire NBRI mean index value change over time.

The NBRI can also be used to generate a metric for fire severity known as the ΔNBR, which can be simply expressed as the change or differential in NBRI over time, typically calculated from the imagery of pre- and post-fire environments and used to determine burn severity. Based on the normalised values of the NBRI, it is divided into seven categories of burn severity and regrowth as seen in Table 10 below.

Table 10: Categories of burn severity for the ΔNBR. Adapted from Escuin et al. (2008).

ΔNBR	Burn Severity
< -0.25	High post-fire regrowth
-0.25 to -0.1	Low post-fire regrowth
-0.1 to +0.1	Unburned
0.1 to 0.27	Low-severity burn
0.27 to 0.44	Moderate-low severity burn
0.44 to 0.66	Moderate-high severity burn
> 0.66	High-severity burn

While the ΔNBR is most commonly applied to the images closest in time to the fire event, it can also be applied to additional images after the fire event, to monitor the degree of regrowth that the ecosystem is undergoing. However, the results from closer to the fire period are more relevant to and accurate at describing burn severity. This process can be utilised until the ecosystem regenerates to pre-fire conditions, at which point the ΔNBR can no longer detect the presence of a

fire. Since the NBRI was calculated for both the pre-/post-fire imagery and the background imagery, it was possible to also determine the ΔNBR for each of the fire events at varying points across the regeneration of the ecosystems. As such, ΔNBR was measured for the mid-fire images and three post-fire images for each fire event.

The Carinda Rd fire event shows the most severe burn intensity of the four events analysed, with an initial ΔNBR of 0.533 for the mid-fire image, which placed it in the moderate-high severity burn category. In the first post-fire image, the ΔNBR decreased to 0.492, still in the moderate-high category, but showing signs of regeneration. These results are displayed graphically in Figure 9 below.

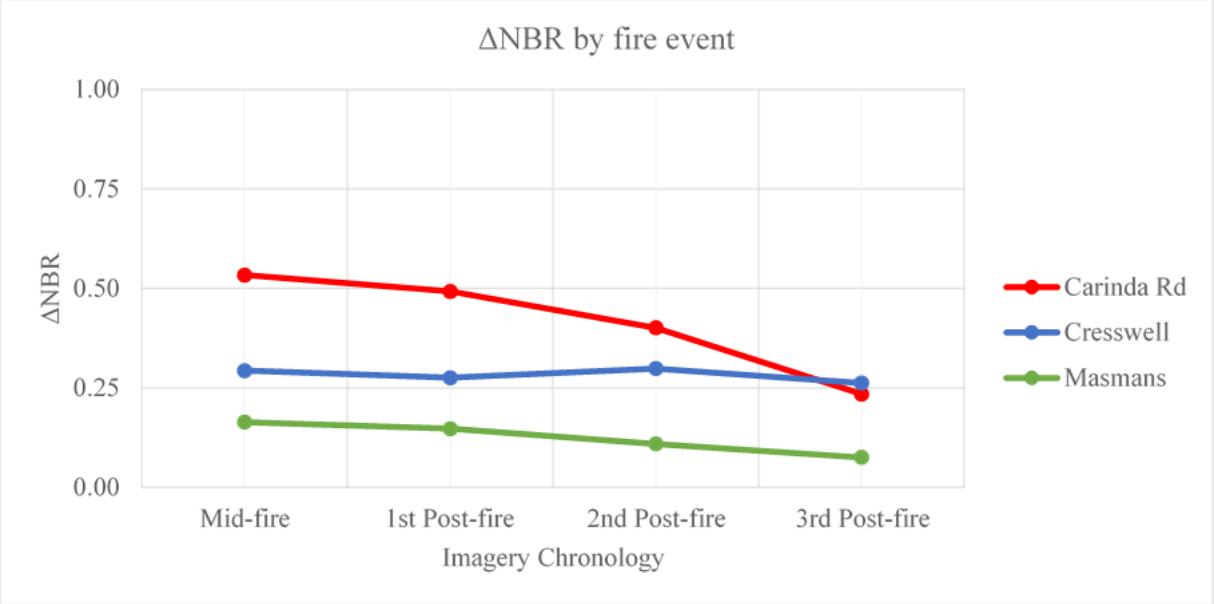

Figure 9: ΔNBR profile for each fire event.

The second post-fire image decreases again to 0.402, which drops a category to moderate-low severity. Finally, the third post-fire image decreases yet again to 0.235, which drops a category further to low-severity. The Cresswell fire event yielded the most unstable profile of the four events, displaying some variation between the first and third post-fire images. The mid-fire image recorded a ΔNBR of 0.293, classifying it as a moderate-low severity burn. This was followed by a minor decrease in the first post-fire image to a ΔNBR 0.276, which places it in the same category. The second post-fire image measured an increase in ΔNBR to 0.299, which was higher than the initial mid-fire figure, but still in the moderate-low severity category. This was followed by a decrease in ΔNBR to 0.262 in the third post-fire image, moving it down a category to low-severity. The Masmans fire event has a less severe burn intensity when compared to some of the other fire events with an initial ΔNBR of 0.164 for the mid-fire image, which placed it in the low severity category. Unlike the Carinda Rd fire, the degree of regeneration across the same period of time was

not as significant in magnitude and followed a more linear progression. The first post-fire image showed a decrease in ΔNBR to 0.147, which was followed by a further decrease to 0.109 in the second post-fire image, both of which were still classified in the low-severity category. The third post-fire image showed another decrease in ΔNBR to 0.075, which reclassified the area as unburned, suggesting that the area is largely regenerated to pre-fire conditions by measure of its vegetation cover.

SATVI

While the SATVI only displayed a > 0.25 variation in index value across the entire profile, the standardised difference between the pre-fire and mid-fire image was close in magnitude to the indices that had much higher overall variation, such as the EVI2, GNDVI, and NBRI. The SATVI also exhibited a subtler post-fire regeneration profile than many of the other high performing indices, which was apparent in all the fire events. Like the other indices, the SATVI recorded its most significant change between the pre-fire and mid-fire images, with a decrease of 0.163 in the Carinda Rd fire, 0.164 in the Cresswell fire, and 0.106 in the Masmans fire. In contrast to the other indices, however, the degree of absolute change between the fire events is much more similar, which would indicate that the SATVI isn't as responsive to burn severity as some other indices but can still detect burned areas quite accurately. The SATVI also proved to be a useful indicator for degree of difference between the burned area and the background area, with mid-fire and post-fire values being consistently different from the background values in the same observation period. This suggest that the SATVI would be a useful tool for large scale applications, where the exact fire boundary is not known and needs to be discerned from a noisy background. These results are displayed graphically in Figure 10 below.

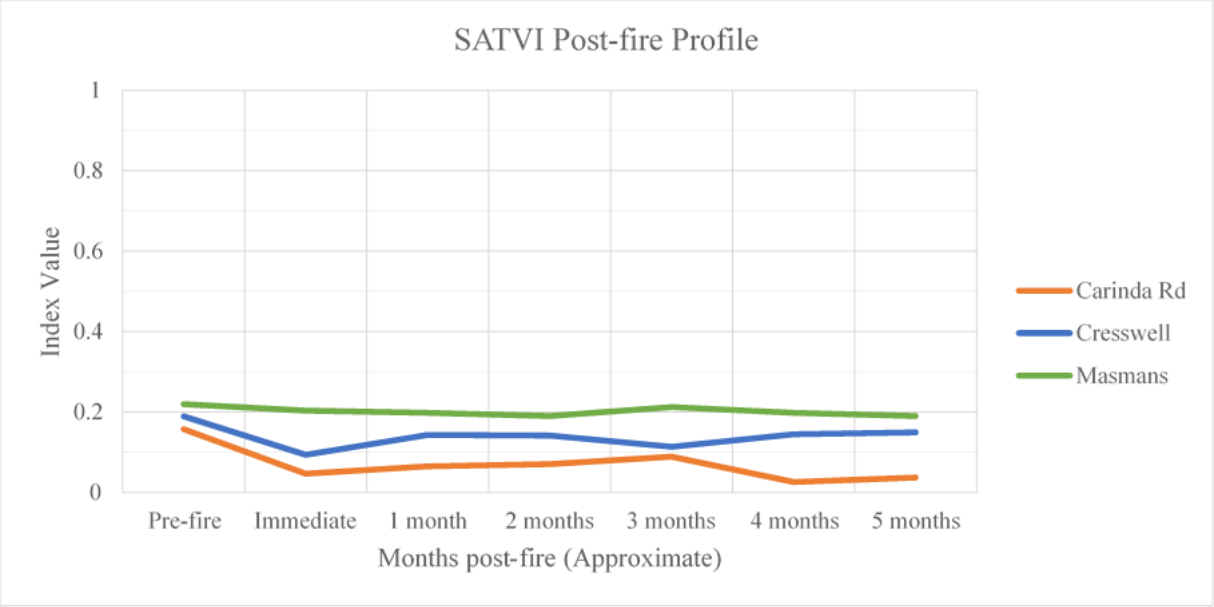

Figure 10: Comparison of post-fire SATVI mean index value change over time.

Recovery of Vegetation Determined by Extended Term Analysis

While the results show that significant vegetation regrowth occurs in wetland environments within one or two months of a fire event occurring, an extended term analysis was undertaken, which revealed the lasting effects of fires over a greater timespan (~1 year). However, due to the length of the period of analysis, it is important to consider the role of seasonality/phenology on vegetation prevalence. To control for this, the same indices were calculated across the entirety of the Northern Marshes as a form of background data, and the results from within the fire boundary were compared to these results. The period it took for post-fire environments to return to pre-fire conditions varied between each fire event, and between each index used for measurement, but in most cases, the data showed that post-fire environments regenerated to pre-fire conditions by measure of most indices within a year. Figure 9 below displays the percentage of indices regenerated to greater than or equal to the pre-fire value, over time. While the indices may indicate that the ecosystem has regenerated to pre-fire conditions, there are numerous variables and determinants of environmental capacity that cannot be directly assessed by some of these indices alone. Factors such as vegetation height and density, soil nutrient capacity, and biodiversity are important metrics of environmental health that cannot be accurately measured by these indices, and therefore must be analysed through other means. Other indices such as the leaf area index, other methods of remote sensing such as lidar and radar, or ground studies should be used to supplement the findings of the indices when making an assessment of ecosystem regeneration in order to achieve an accurate result.

Carinda Rd Fire

The extended term analysis of the Carinda Rd fire event shows the eventual return of the area to pre-fire conditions in regard to a majority of the spectral indices, but with differing rates of regeneration for many of them. Amongst the spectral indices utilised for the analysis, the mean return time to pre-fire conditions for the Carinda Rd fire was approximately 144 days, with a minimum return time of ~ 96 days as reported by the NDWI2, SLAVI, & SR, and a maximum return time that wasn't recorded in the observation period by the MNDWI. The next longest regenerative period was ~ 224 days, as reported by the SATVI. All indices showed a constant progression away from post-fire conditions for the entire analysis period except for EVI2, which decreased again at ~ 288 days post-fire. A complete list of the return times for each index can be viewed in Table 11 on page 41, and a visual representation of the profile in Figure 11 below. Despite being the largest and most severe fire of the three events analysed, the Carinda Rd fire exhibits the lowest mean return time to pre-fire values, which would indicate that it was the fastest regenerating post-fire ecosystem. It is important to note that this regrowth is only immature

vegetation and does not indicate that the ecosystem has completely regenerated to its pre-fire conditions.

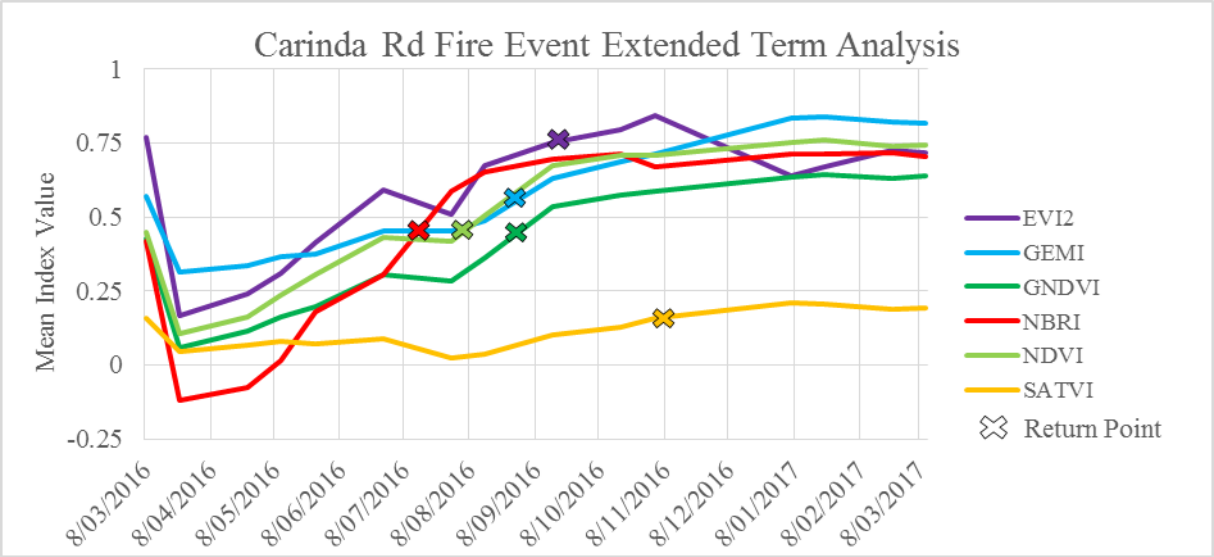

Figure 11: Return to pre-fire conditions profile for six key indices after Carinda Rd fire (15/03/16 – 26/03/16).

Cresswell Fire

The Cresswell fire event extended term analysis shows on average a longer return to pre-fire levels when compared to the Carinda Rd fire event, even though the ΔNBR indicated that it was a less severe burn. Average return time was approximately 212 days, with a minimum of ~ 184 days as measured by the NDWI2 and SLAVI, and a maximum of 248 days as reported by the EVI2 and SATVI. Sixty-eight percent of the indices experienced a decrease at ~344 days post-fire, rising to 95% by 360 days post-fire. This is most likely attributable to seasonal variation heading into autumn, or from other external factors unrelated to the fire event. However, the younger vegetation of the recently burned area may be less hardy, causing it to be more susceptible to environmental change. The Cresswell fire event saw the longest average return time to pre-fire values, taking almost four months longer than the Carinada Rd fire event and one month longer than the Masmans fire event for post-fire ecosystem regeneration to return the environment to its previous state. A complete list of the return times for each index can be viewed in Table 11 on page 41, and a visual representation of the profile in Figure 12 on the next page.

Masmans Fire

The Masmans fire event, while having the lowest ΔNBR of the three fire events, exhibited the most variable return time results of the fire events, and many indices exhibited oscillations above and below pre-fire values towards the end of the profile. The average return time to pre-fire values was approximately 178 days, with a minimum of ~ 107 days as reported by the CTVI, EVI2, MNDWI, MSAVI, NDVI, NRVI, RVI, SR, TVI, and TTVI and a maximum of ~ 315 days as reported by the DVI, GEMI, SAVI, and WDVI. By 251 days, 72% of the indices had reverted to pre-fire values,

and by 315 days, 86% of indices has reverted. There were two periods in which > 95% of the indices regressed to worse values than the previous, once at ~ 154 days post-fire, and once at ~ 267 – 283 days post-fire. The Masmans fire event, while the smallest and the least severe, was only the second fastest to regenerate, and saw the highest variability in return times. A complete list of the return times for each index can be viewed in Table 11 on the next page, and a visual representation of the profile in Figure 13 below.

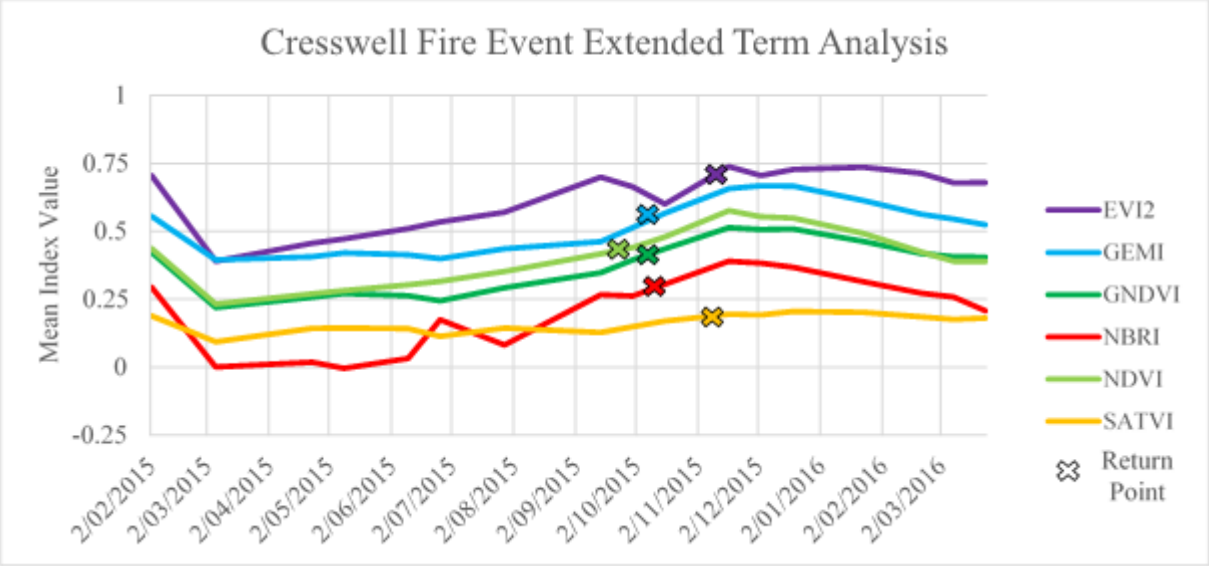

Figure 12: Return to pre-fire conditions profile for six key indices after Cresswell fire (25/02/15 – 14/03/15).

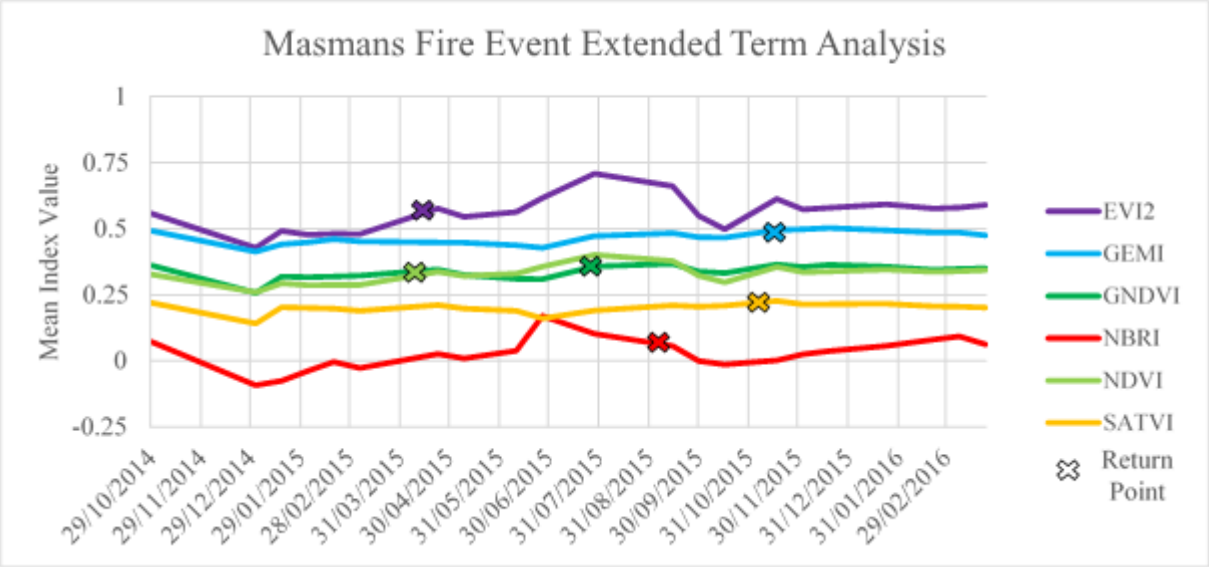

Figure 13: Return to pre-fire conditions profile for six key indices after Masmans fire (29/12/14 – 06/01/15).

Table 11: Time taken for each index to return to its mean pre-fire value by fire event.

	Carinda Rd	**Cresswell**	**Masmans**
CTVI	144	200	107
DVI	176	216	315
EVI	176	216	203
EVI2	208	248	107
GEMI	176	216	315
GNDVI	176	216	251
MNDWI	No return	240	107
MSAVI	144	216	107
MSAVI2	176	216	203
NBRI	128	216	171
NDVI	144	200	107
NDWI	176	216	251
NDWI2	96	184	155
NRVI	144	200	107
RVI	144	200	107
SATVI	224	248	315
SAVI	176	216	203
SLAVI	96	184	155
SR	96	200	107
TVI	144	200	107
TTVI	144	200	107
WDVI	176	216	315

2.4.4 Detection of Burned Areas based on Classification

Unsupervised Classification

The K-means/Iso-Cluster unsupervised classification method was fairly consistent when applied across the pre-/post-fire environments but failed to show any measurable response to the fire events occurring, as can be seen in Figure 14 below. It also lacked the discerning ability of some of the supervised classifications, frequently misclassifying areas of diverse vegetation cover by grouping together multiple different vegetation species as one class or combining open field and paddocks with shrubland vegetation. These different land types were generally more accurately classified by the supervised classification methods, which were better suited to identifying the spectral differences between the different land cover types present in the scene. Additionally, the composition of the unsupervised classification within the fire boundary showed no significant changes between the pre- and post-fire images, suggesting that the active fire event and burn scar were not spectrally unique enough amongst the rest of the scene to allow them to be classified as a separate class. The burn scars were frequently misclassified as various land cover types, indicating the lack of spectral diversity present in burned areas to elicit a unique class designation from the unsupervised classifier. Previous research by Miller & Yool (2002) notes the difficulty in using an unsupervised classification to detect burn scars in woodland ecosystems when compared to a trained supervised classification, albeit with a much smaller difference in accuracy. Figure 10 below shows the unsupervised classifications of the first post-fire image compared to the indicated fire boundary, which clearly exhibits a misclassification of the fire area.

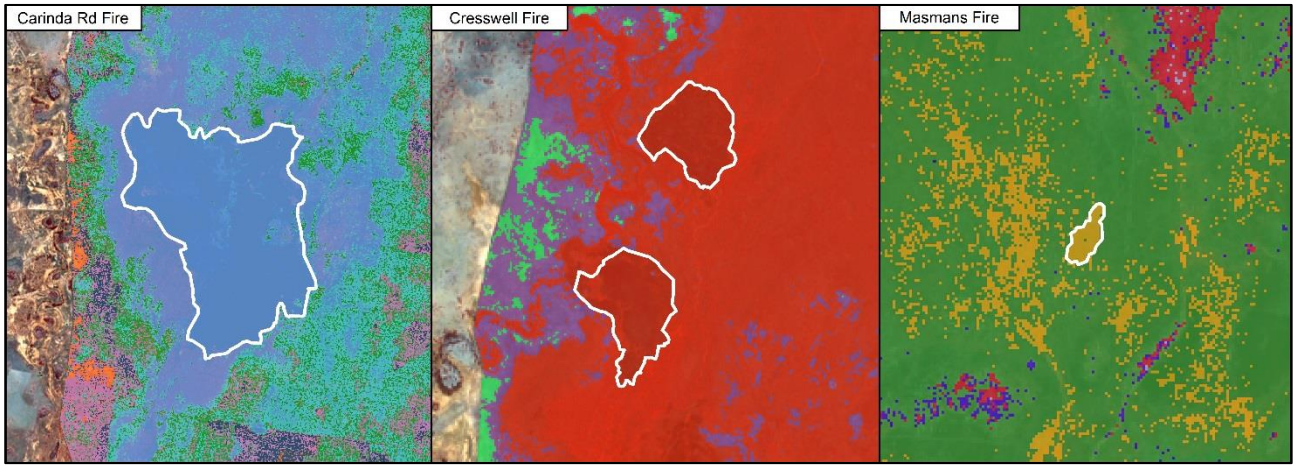

Figure 14: Comparison of post-fire unsupervised classifications for the three fire events.

Supervised Classification

Neural Networks

The neural networks classifier was the least consistent of the three supervised classification methods tested, displaying erratic changes in classification accuracy between images of the same fire event that were no more than a month apart, and also failed to classify burned pixels at all in the post-fire image of the Masmans fire. It consistently generalised classes across large areas of non-homogenous land cover and failed to properly discern burned pixels in scenes where the other classifications did. Figure 15 below displays the change in burned pixel identification by the Neural Networks classifier for the Carinda Rd fire over a period of approximately two months.

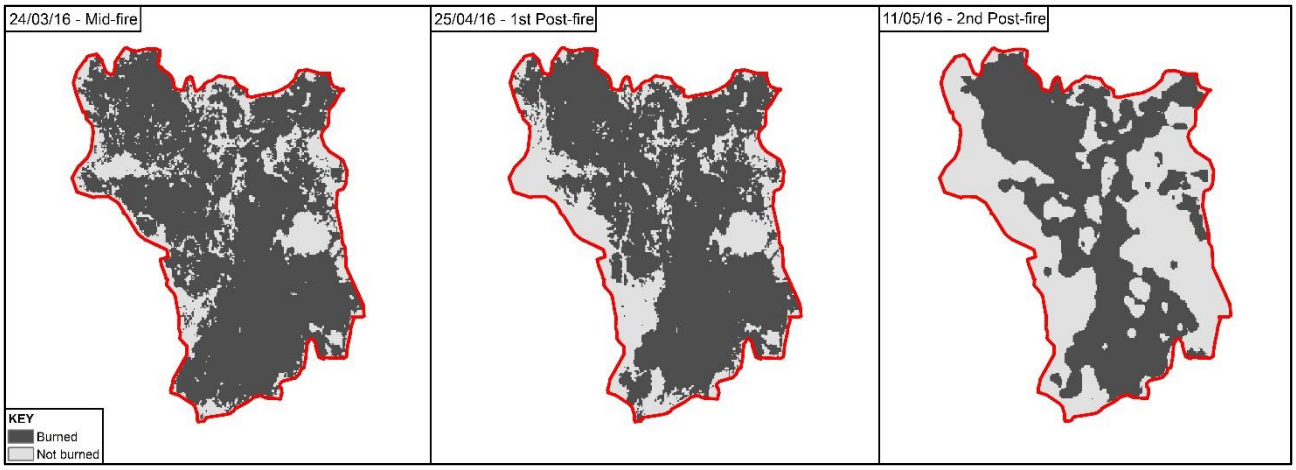

Figure 15: Changed in burned pixel classification for Neural Networks classifier over time.

The average commission error rate was 13.97% for the Carinda Rd fire event and 34.99% for the Cresswell fire event. The Masmans fire event was excluded from the average as no burned pixels were detected in any of the post-fire imagery for the Masmans event. This resulted in an overall commission error rate of 24.48%, which suggests that the neural net classifier was only moderately accurate at identifying the signature of burned areas in the context of their surroundings. The upward trend in the Carinda Rd fire event from 0.14% in the mid-fire image to 28.39% in the third post-fire image indicates that the burned areas are becoming more spectrally heterogeneous as regrowth occurs, which could confuse the classifier. The higher accuracy result of the Carinda Rd fire event compared to the Cresswell and Masmans events may indicate that the Carinda Rd event was a more severe and complete burn, resulting in a burned area that was significantly different to unburned areas and therefore easier to classify.

The average omission error rate was 35.43% for the Carinda Rd fire event and 90.37% for the Cresswell fire event, resulting in an overall omission error rate of 62.90%. The Masmans fire event was again excluded for the reasons mentioned above. The Carinda Rd fire event showed an upward trend similar to the results of the first metric, increasing from 23.91% in the mid-fire image to

49.29% by the second post-fire image, but then decreased to 38.67% in the third image. This suggests that the classification of burned pixels may be becoming less accurate as the burn scars begin to fade and regrowth begins to influence the training process of the classifier. Other pixels inside the fire boundary were generally classified as wetland marsh or water, with these classes increasing in prevalence as the distance from fire increases, indicating the presence of vegetation regrowth.

Random Forest

The random forest classifier fared relatively well with the diverse land coverings present in the study area, commonly providing very high accuracy results for the delineation of burn pixels and generally strong results amongst the rest of the classes overall. Interpolation and generalisation of classes was minimal, sometimes to a fault, inducing pixel noise into the classification, seen as random pixels of different classes interspersed amongst relatively large blocks of another, singular class, which can be observed in Figure 16 below. As such, to properly delineate the full footprint of a burn scar, a smoothing or interpolation algorithm would need to be employed.

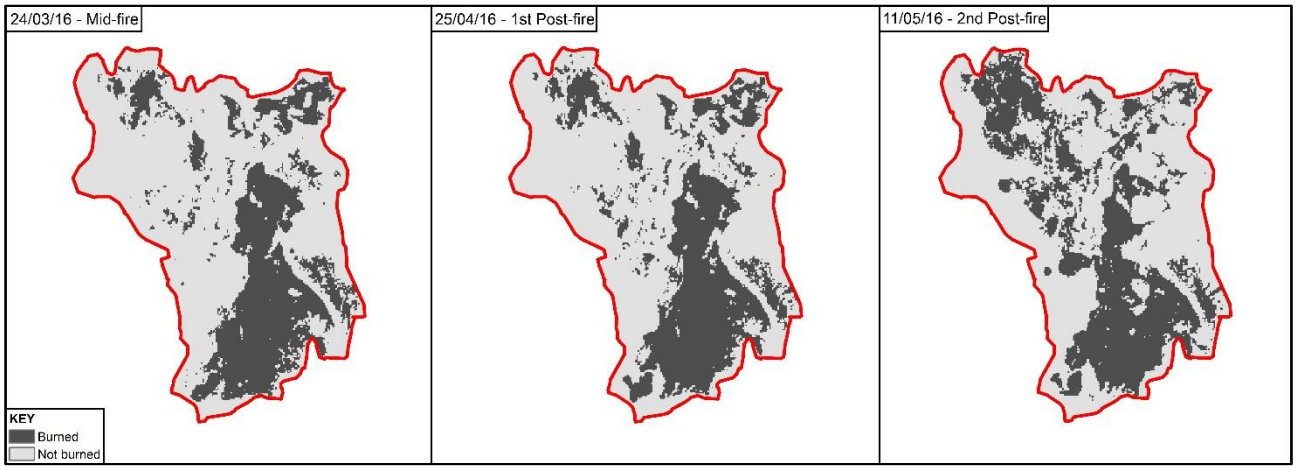

Figure 16: Changed in burned pixel classification for Random Forest classifier over time.

The average commission error rate was 0.06% for the Carinda Rd fire event, 0.36% for the Cresswell fire event, and 98.79% for the Masmans fire event, resulting in an overall commission error rate of 33.35%. The significantly high results of the Carinda Rd and Cresswell fire events suggests that the Random Forest classifier was well suited to identifying the unique spectral signature of the burned areas, and accurately discern the burn pixels from a mixture of surrounding land cover types, resulting in essentially no false positive results across the two events. This level of accuracy was not withheld through the Masmans fire event, however, which experienced a very high commission error rate, which suggests the classifier was confused. This is most likely due to the Masmans fire event being smaller and less severe, thus leaving a less well-defined burn scar that was overtaken by regenerating vegetation faster than the other events.

The average omission error rate was 64.26% for the Carinda Rd fire event, 69.49% for the Cresswell fire event, and 33.95% for the Masmans fire event, resulting in an overall omission error rate of 50.90%. These results are quite inaccurate in comparison to the accuracy indicated by the first metric, and also when compared to the results of the SVM classifier and seems to be the result of the misclassification of numerous pixels scattered throughout the fire boundary area, culminating in a 'noisy' classification. This occurs frequently with large swathes of burned areas being interrupted by pixels misclassified as wetland marsh or water. Additionally, the decreasing omission error rate from 68.19% in the mid-fire image to 58.61% in the third post-fire image would suggest that these speciously classified pixels are a result of the fading burn scar and vegetation regrowth.

Support Vector Machine

Previous studies have also used the SVM classifier for mapping burn scars to significant success, such as in the study by (George P. Petropoulos et al., 2011), which found that diverse kernel function implementation of SVM was up to 98.57% accurate at delineating burn scars in Mediterranean grassland ecosystems from immediate post-fire imagery. However, this type of environment and the composition of its vegetation is drastically different to a wetland environment, and typically slower to regenerate, resulting in a more defined burn scar that would be easier to detect with remote sensing methodologies. Additionally, this study only utilised a uni-temporal approach, and therefore did not test the capabilities of SVM for measuring the behaviour of burn scars over time The support vector machine classification was the least efficient in terms of classifier training and execution time, frequently taking multiple hours to complete, but saw strong performance in both of the metrics used for analysis, allowing it to edge out random forest as the most accurate classifier overall.

The average commission error rate was 3.33% for the Carinda Rd fire event, 2.68% for the Cresswell fire event, and 93.91% for the Masmans fire event, culminating in an overall commission error rate of 30.31%. It can be concluded that the SVM classifier was well equipped to identify the spectral signature of the Carinda Rd and Cresswell burn scars, but the smaller, less severe burn scar of the Masmans fire proved problematic, resulting in a high commission error. This suggests that like the other supervised classifiers, the SVM benefits from a larger, more spectrally different burn scar for the accurate classifications of burned areas.

The average omission error rate was 34.81% for the Carinda Rd fire event, 63.65% for the Cresswell fire event, and 26.74% for the Masmans fire event, culminating in an overall omission error rate of 41.73%. The SVM was the strongest performer in this metric consistently providing more accurate results than the supervised classifiers, which indicates that it is less prone to the misclassification of small groups of pixels like the random forest classifier, and therefore, by extension, more suitable for detecting more complete burn scars. Figure 17 below shows the change in burned pixel identification by the Support Vector Machines classifier for the Carinda Rd fire over approximately two months.

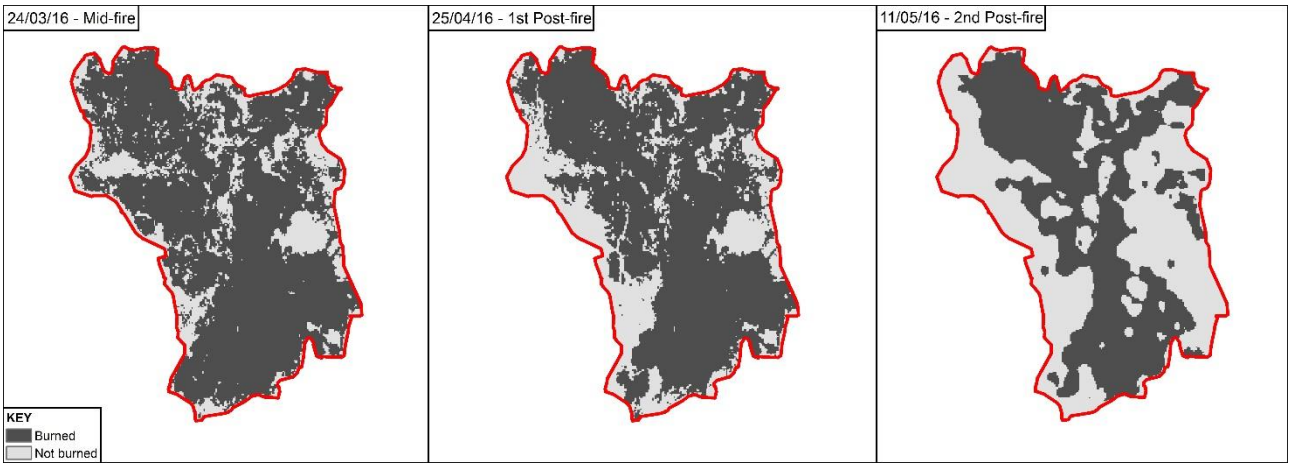

Figure 17: Changed in burned pixel classification for Support Vector Machine classifier over time.

2.5 Evaluation and Conclusion

The most accurate spectral indices for mapping burn scars in wetlands tended to be those that utilised the red, green, and infrared bands with some known constants and coefficients to make an indirect measurement of vegetation cover, such as the GNDVI, the NBRI, the EVI2, and the SATVI. These indices generally showed consistently high Std. dIndex values across all the fire events, proving their capability at detecting fire-induced changes to ground cover. When considering the spectral index profiles, it can be concluded form the analysis that wetland environments typically regenerate to their pre-fire states within a year of the fire event occurring, as can be observed in Figure 18 below, where approximately 75% of indices have a value that is greater than or equal to the pre-fire value by 7 months post-fire. However, these indices cannot determine certain characteristics that are key indicators of ecosystem health and regeneration, such as vegetation maturity and biodiversity, so further information is required to properly determine if the ecosystem has regenerated completely. So, while the post-fire ecosystem may have regenerated to pre-fire conditions based on the use of one index, the only way to derive a more accurate assessment is to use a range of different remote sensing methods and ground studies that analyse the different physical characteristics of wetland environments.

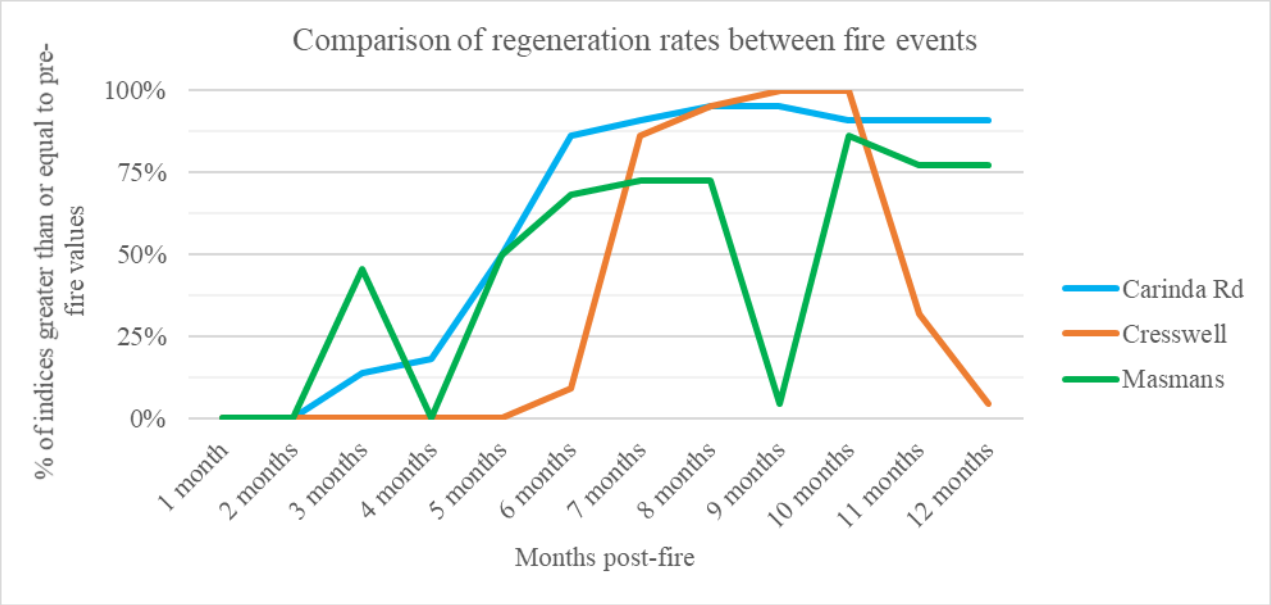

Figure 18: Comparison of time taken for indices to return to pre-fire conditions across the three fire events.

In their comparison of ten classification methods (including neural networks, support vector machine, and classification and regression trees) for burn scar mapping in the Mediterranean, Mallinis & Koutsias (2012) concluded that the difference between the accuracies of each method was largely statistically insignificant, and that considerations such as performance and efficiency would have a greater impact on the final decision of classification method. However, the findings of this paper suggest that in wetland ecosystems, the choice of classification method used will have a greater impact on the accuracy of the results. The most accurate classifications were supervised, particularly the SVM classifier, which provided a good balance between low error and footprint completeness, although comes with the caveat of increased training and classifying time when compared to other methods. While the supervised methods displayed some variability in accuracy both between different fire events and at post-fire periods greater than ~ 1.5 months, they were consistently more accurate at delineating both burned areas and other classes than the unsupervised classification. One of the potential shortcomings of the neural networks and support vector machines classifiers in the ENVI suite is that is doesn't allows for the cross-validation of the classification that is available with the random forest classifier, which would likely influence the overall accuracy of the classification and eliminate erroneous classifications.

One of the objectives of this paper is to translate what was learned about the response of wetlands to bushfire events into practical recommendations and applications that could be applied by environmental managers at varying spatial scales. Based on the results generated by this study, a synthesis of different remote sensing techniques is recommended to complete the burn scar mapping process from identification to competition. Fire identification could be undertaken through various means, such as the Sentinel Hotspot system, the MODIS Active Fires System, or from local

fire reports, but the Sentinel system worked well for this study. Once fires are identified, imagery should be acquired both during, and as soon after the fire event has occurred as possible, so as to be able to assess the full extent of the burn scar without the interference of regrowth. Depending on the size of the fire event, imagery of different spatial resolutions could be used, but for more accurate results, sensors with small pixel sizes, such as the Landsat 8 or Sentinel-2A/B satellites should be preferred. Indices such as the EVI2 or GNDVI could then be performed on the imagery to determine burn extent, and the NBRI/ΔNBR could be used for both extent and severity. The results of these indices could also be used as inputs to train supervised classifiers for a more specific delineation between burned and unburned areas. Due to the diverse selection of variables that influence the characteristics of fires, it is imperative that management strategies be tailored to each event and take a holistic and adaptive approach, with consideration for the surrounding ecosystems.

Ultimately, there are multiple factors to consider when comparing these methods of analysis, and from the data it is evident that the diverse methodologies all have distinct and different advantages and disadvantages.

3. Synthesis

Current projections predict that in the coming years there will be an observable increase in the number of extreme fire days and already severe fire seasons will be prolonged as a result of anthropogenic climate change. These delicate and vital wetland ecosystems, and the biodiversity they foster, will be at greater risk of damage or degradation from bushfire events and being able to utilise the most efficient and effective means of limiting these impacts will become of paramount importance. The role of remote sensing in assessing damage and informing rehabilitation and management efforts will be further developed as new technologies and techniques arise, and more information is gathered about post-fire wetland ecosystems. While there exists significant and comprehensive information into the accuracy and efficiency of diverse remote sensing methods for burn scar delineation in various dryland environments, the information on the efficacy of different remote sensing methods in wetland environments is far more limited, and the unique challenges to remote sensing posed by wetland ecosystems are not fully investigated or understood. The aim of this thesis is to provide a preliminary insight into how current understandings of remote sensing might have to be reconsidered for wetland environments, and what techniques may have to be modified or created to achieve the levels of accuracy gained in measuring burn scars in dryland environments.

3.1 Future Research Directions

There are numerous and diverse potential avenues for continuing this research, including modifying the methodologies already used or adding new techniques, analysing burn scars over longer periods of time to obverse possible longer lasting effects, and expanding the analysis into similar wetland study areas, both within Australia and globally. The methodology used in this study should be more broadly applicable to wetlands of similar structure in terms of vegetation composition and inundation regime. One such example is the Gwydir Wetlands, which is located some 230 km to the north-east of the Macquarie Marshes, which is an area comparable to the Macquarie Marshes in terms of vegetation, hydrology, and fire history. The Gwydir Wetlands are also Rasmsar listed, indicating their environmental significance and the desire to limit the amount of damage occurring from bushfires.

Other potential future research avenues include the monitoring of other key environmental variables in post-fire environments, which if left unmanaged, can cause severe and lasting degradation of the ecosystem, potentially resulting in a shift in total ecosystem capability. An example of this is soil erosion arising from vegetation loss, which can be highly detrimental to ecosystems, and can be monitored remotely through multispectral satellite imagery. This could be combined with a

comparison of spectral index profiles and vegetation community mapping, which would allow for a targeted approach of the species that are more severely impacted by fire events. This will also allow for the monitoring of species that are dependent on fire for growth and determine whether these communities are being burnt frequently enough to stimulate the proper amount of growth.

Ideally, a synthesis of the methodologies used in this study could be adopted to measure burn scars in wetlands at much broader spatial scales, so as to further inform already existing global fire monitoring systems, but with greater accuracy and finer resolution. In the interests of increasing accuracy and efficiency, the entire process could also be semi- or fully automated, with an output product that could be updated almost continuously. This could be achieved through one of the recently established collaborative supercomputer networks, such as the Australian Data Cube, which would allow for the broader dissemination of information to researchers and managers, as well as allow for community development.

References

Aber, J. S., Pavri, F., & Aber, S. (2012). *Wetland Environments: A Global Perspective*. John Wiley & Sons.

Baret, F., & Guyot, G. (1991). Potentials and limits of vegetation indices for LAI and APAR assessment. Remote Sensing of Environment, 35(2), 161–173. https://doi.org/10.1016/0034-4257(91)90009-U

Birth, G. S., & McVey, G. R. (1968). Measuring the Color of Growing Turf with a Reflectance Spectrophotometer. *Agronomy Journal*, *60*(6), 640–643. https://doi.org/10.2134/agronj1968.00021962006000060016x

Boer, M. M., Macfarlane, C., Norris, J., Sadler, R. J., Wallace, J., & Grierson, P. F. (2008). Mapping burned areas and burn severity patterns in SW Australian eucalypt forest using remotely-sensed changes in leaf area index. *Remote Sensing of Environment*, *112*(12), 4358–4369. https://doi.org/10.1016/j.rse.2008.08.005

Bolten, J. D., Lakshmi, V., & Njoku, E. G. (2003). Soil moisture retrieval using the passive/active L- and S-band radar/radiometer. *IEEE Transactions on Geoscience and Remote Sensing*, *41*(12), 2792–2801. https://doi.org/10.1109/TGRS.2003.815401

Bourgeau-Chavez, L. L., Kasischke, E. S., Brunzell, S., Mudd, J. P., & Tukman, M. (2002). Mapping fire scars in global boreal forests using imaging radar data. *International Journal of Remote Sensing*, *23*(20), 4211–4234. https://doi.org/10.1080/01431160110109589

Breiman, L. (2001). Random Forests. *Machine Learning*, *45*(1), 5–32. https://doi.org/10.1023/A:1010933404324

Brumby, S. P., Theiler, J. P., Bloch, J. J., Harvey, N. R., Perkins, S. J., Szymanski, J. J., & Young, A. C. (2002). Evolving land cover classification algorithms for multispectral and multitemporal imagery. *Proceedings of SPIE*, *4480*, 120–129.

Cassidy, L. (2007). Mapping the annual area burned in the wetlands of the Okavango panhandle using a hierarchical classification approach. *Wetlands Ecology and Management*, *15*(4), 253–268. https://doi.org/10.1007/s11273-006-9026-2

Chen, W., Moriya, K., Sakai, T., Koyama, L., & Cao, C. X. (2016). Mapping a burned forest area from Landsat TM data by multiple methods. *Geomatics, Natural Hazards and Risk*, *7*(1), 384–402. https://doi.org/10.1080/19475705.2014.925982

Chuvieco, E., Martín, M. P., & Palacios, A. (2002). Assessment of different spectral indices in the red-near-infrared spectral domain for burned land discrimination. *International Journal of Remote Sensing*, *23*(23), 5103–5110. https://doi.org/10.1080/01431160210153129

Civco, D. L. (1993). Artificial neural networks for land-cover classification and mapping. *International Journal of Geographical Information Systems*, *7*(2), 173–186. https://doi.org/10.1080/02693799308901949

Collett, E. (2005). *Field Guide to Polarization* (Illustrated, Vol. 5). Society of Photo Optical.

Crist, E. P., & Cicone, R. C. (1984). A Physically-Based Transformation of Thematic Mapper Data—The TM Tasseled Cap. *IEEE Transactions on Geoscience and Remote Sensing*, *GE-22*(3), 256–263. https://doi.org/10.1109/TGRS.1984.350619

Deering, D. W., Rouse Jr, J. W., Haas, R. H., & Schell, J. A. (1975). Measuring "forage production" of grazing units from Landsat MSS data. Proceedings of 10th International Symposium on Remote Sensing of Environment, 1169–1178.

Delegido, J., Verrelst, J., Alonso, L., & Moreno, J. (2011). Evaluation of Sentinel-2 Red-Edge Bands for Empirical Estimation of Green LAI and Chlorophyll Content. *Sensors (Basel, Switzerland)*, *11*(7), 7063–7081. https://doi.org/10.3390/s110707063

Department of the Environment and Energy. (2009, August 29). The Ramsar Convention on Wetlands [Text]. Retrieved 8 October 2017, from http://www.environment.gov.au/

Ding, F., Zhang, X., Fan, P., & Chen, L. (2012). A new method for burnt scar mapping using spectral indices combined with Support Vector Machines. In *2012 First International Conference on Agro- Geoinformatics (Agro-Geoinformatics)* (pp. 1–4). https://doi.org/10.1109/Agro-Geoinformatics.2012.6311662

Dubois, P. C., Zyl, J. van, & Engman, T. (1995). Measuring soil moisture with imaging radars. *IEEE Transactions on Geoscience and Remote Sensing*, *33*(4), 915–926. https://doi.org/10.1109/36.406677

Durden, S. L., Zyl, J. J. van, & Zebker, H. A. (1989). Modeling and observation of the radar polarization signature of forested areas. *IEEE Transactions on Geoscience and Remote Sensing*, *27*(3), 290–301. https://doi.org/10.1109/36.17670

Dymond, C. C., Mladenoff, D. J., & Radeloff, V. C. (2002). Phenological differences in Tasseled Cap indices improve deciduous forest classification. *Remote Sensing of Environment*, *80*(3), 460–472. https://doi.org/10.1016/S0034-4257(01)00324-8

Elmore, A. J., Mustard, J. F., Manning, S. J., & Lobell, D. B. (2000). Quantifying Vegetation Change in Semiarid Environments: Precision and Accuracy of Spectral Mixture Analysis and the Normalized Difference Vegetation Index. *Remote Sensing of Environment*, *73*(1), 87–102. https://doi.org/10.1016/S0034-4257(00)00100-0

Escuin, S., Navarro, R., & Fernández, P. (2008). Fire severity assessment by using NBR (Normalized Burn Ratio) and NDVI (Normalized Difference Vegetation Index) derived from LANDSAT TM/ETM images. *International Journal of Remote Sensing*, *29*(4), 1053–1073. https://doi.org/10.1080/01431160701281072

European Space Agency (ESA). (2017). Sentinel-1 - ESA EO Missions - Earth Online - ESA. Retrieved 7 October 2017, from https://earth.esa.int/web/guest/missions/esa-operational-eo-missions/sentinel-1

Evans, D. L., Farr, T. G., Ford, J. P., Thompson, T. W., & Werner, C. L. (1986). Multipolarization Radar Images for Geologic Mapping and Vegetation Discrimination. *IEEE Transactions on Geoscience and Remote Sensing*, *GE-24*(2), 246–257. https://doi.org/10.1109/TGRS.1986.289644

Fernandez-Manso, A., Quintano, C., & Roberts, D. A. (2016). Burn severity influence on post-fire vegetation cover resilience from Landsat MESMA fraction images time series in

Mediterranean forest ecosystems. *Remote Sensing of Environment*, *184*, 112–123. https://doi.org/10.1016/j.rse.2016.06.015

Gao, B. (1996). NDWI—A normalized difference water index for remote sensing of vegetation liquid water from space. *Remote Sensing of Environment*, *58*(3), 257–266. https://doi.org/10.1016/S0034-4257(96)00067-3

Gill, A. M., Woinarski, J., York, A., Australia, Environment Australia, Australia, & Department of the Environment and Heritage. (1999). *Australia's biodiversity--responses to fire: plants, birds, and invertebrates*. Canberra, ACT: Dept. of the Environment and Heritage.

Gislason, P. O., Benediktsson, J. A., & Sveinsson, J. R. (2004). Random Forest classification of multisource remote sensing and geographic data. In *IGARSS 2004. 2004 IEEE International Geoscience and Remote Sensing Symposium* (Vol. 2, pp. 1049–1052 vol.2). https://doi.org/10.1109/IGARSS.2004.1368591

Gislason, P. O., Benediktsson, J. A., & Sveinsson, J. R. (2006). Random Forests for land cover classification. *Pattern Recognition Letters*, *27*(4), 294–300. https://doi.org/10.1016/j.patrec.2005.08.011

Goodwin, N. R., Collett, L. J., Denham, R. J., Flood, N., & Tindall, D. (2013). Cloud and cloud shadow screening across Queensland, Australia: An automated method for Landsat TM/ETM + time series. *Remote Sensing of Environment*, *134*, 50–65. https://doi.org/10.1016/j.rse.2013.02.019

Graham, S. (1999, September 17). Remote Sensing : Feature Articles [Text.Article]. Retrieved 6 October 2017, from https://earthobservatory.nasa.gov/Features/RemoteSensing/remote_08.php

Haywood, A., Verbesselt, J., & Baker, P. J. (2016). Mapping Disturbance Dynamics in Wet Sclerophyll Forests Using Time Series Landsat. *ISPRS - International Archives of the Photogrammetry, Remote Sensing and Spatial Information Sciences*, *XLI-B8*, 633–641. https://doi.org/10.5194/isprsarchives-XLI-B8-633-2016

Hensley, S., Chapin, E., Freedman, A., Le, C., Madsen, S., Michel, T., … Wheeler, K. (2001). First P-band results using the GeoSAR mapping system. *Geoscience and Remote Sensing Symposium, 2001. IGARSS '01. IEEE 2001 International*, *1*, 126–128 vol.1. https://doi.org/10.1109/IGARSS.2001.976078

Holden, Z. A., Smith, A. M. S., Morgan, P., Rollins, M. G., & Gessler, P. E. (2005). Evaluation of novel thermally enhanced spectral indices for mapping fire perimeters and comparisons with fire atlas data. *International Journal of Remote Sensing*, *26*(21), 4801–4808. https://doi.org/10.1080/01431160500239008

Horning, N., Leutner, B., & Wegmann, M. (2016). Land Cover or Image Classification Approaches. In *Remote Sensing and GIS for Ecologists Using Open Source Software*. Exeter, UK: Pelagic Publishing.

Huete, A. R. (1988). A soil-adjusted vegetation index (SAVI). Remote Sensing of Environment, (3), 295–309.

Jiang, Z., Huete, A. R., Didan, K., & Miura, T. (2008). Development of a two-band enhanced vegetation index without a blue band. *Remote Sensing of Environment*, *112*(10), 3833–3845. https://doi.org/10.1016/j.rse.2008.06.006

Jin, S., & Sader, S. A. (2005). Comparison of time series tasseled cap wetness and the normalized difference moisture index in detecting forest disturbances. *Remote Sensing of Environment*, *94*(3), 364–372. https://doi.org/10.1016/j.rse.2004.10.012

Kasischke, E. S., Melack, J. M., & Craig Dobson, M. (1997). The use of imaging radars for ecological applications—A review. *Remote Sensing of Environment*, *59*(2), 141–156. https://doi.org/10.1016/S0034-4257(96)00148-4

Klemas, V. (2011). Remote Sensing of Wetlands: Case Studies Comparing Practical Techniques. *Journal of Coastal Research*, 418–427. https://doi.org/10.2112/JCOASTRES-D-10-00174.1

Knipling, E. B. (1970). Physical and physiological basis for the reflectance of visible and near-infrared radiation from vegetation. *Remote Sensing of Environment*, *1*(3), 155–159. https://doi.org/10.1016/S0034-4257(70)80021-9

Kontoes, C. C., Poilvé, H., Florsch, G., Keramitsoglou, I., & Paralikidis, S. (2009). A comparative analysis of a fixed thresholding vs. a classification tree approach for operational burn scar detection and mapping. *International Journal of Applied Earth Observation and Geoinformation*, *11*(5), 299–316. https://doi.org/10.1016/j.jag.2009.04.001

Kotsiantis, S. B. (2007). Supervised Machine Learning: A Review of Classification Techniques. In I. Zaharakis & P. Pintelas, *Frontiers in Artificial Intelligence and Applications* (Vol. 160, pp. 3–24).

Kotze, D. C. (2013). The effects of fire on wetland structure and functioning. *African Journal of Aquatic Science*, *38*(3), 237–247. https://doi.org/10.2989/16085914.2013.828008

Lentile, L. B., Holden, Z. A., Smith, A. M. S., Falkowski, M. J., Hudak, A. T., Morgan, P., … Benson, N. C. (2006). Remote sensing techniques to assess active fire characteristics and post-fire effects. *International Journal of Wildland Fire*, *15*(3), 319–345.

Leutner, B., & Horning, N. (2017, April 15). Tools for Remote Sensing Data Analysis (RSToolbox). CRAN. Retrieved from https://cran.r-project.org/web/packages/RStoolbox/RStoolbox.pdf

Liaw, A., & Wiener, M. (2015, October 7). Breiman and Cutler's Random Forests for Classification and Regression (randomForest). Retrieved from http://www.piotrkosoft.com/pub/Linux/software/mirrors/CRAN/web/packages/RRF/RRF.pdf

Lichtenthaler, H. K., Wenzel, O., Buschmann, C., & Gitelson, A. (1998). Plant Stress Detection by Reflectance and Fluorescencea. Annals of the New York Academy of Sciences, 851(1), 271–285. https://doi.org/10.1111/j.1749-6632.1998.tb09002.x

Ling, F., Du, Y., Zhang, Y., Li, X., & Xiao, F. (2015). Burned-Area Mapping at the Subpixel Scale With MODIS Images. *IEEE Geoscience and Remote Sensing Letters*, *12*(9), 1963–1967. https://doi.org/10.1109/LGRS.2015.2441135

Loboda, T. V., Hoy, E. E., Giglio, L., & Kasischke, E. S. (2011). Mapping burned area in Alaska using MODIS data: a data limitations-driven modification to the regional burned area algorithm. *International Journal of Wildland Fire*, *20*(4), 487–496.

Lu, D., & Weng, Q. (2007). A survey of image classification methods and techniques for improving classification performance. *International Journal of Remote Sensing*, *28*(5), 823–870. https://doi.org/10.1080/01431160600746456

Lucas, R., Armston, J., Fairfax, R., Fensham, R., Accad, A., Carreiras, J., … Shimada, M. (2010). An Evaluation of the ALOS PALSAR L-Band Backscatter - Above Ground Biomass Relationship Queensland, Australia: Impacts of Surface Moisture Condition and Vegetation Structure. *IEEE Journal of Selected Topics in Applied Earth Observations and Remote Sensing*, *3*(4), 576–593. https://doi.org/10.1109/JSTARS.2010.2086436

Lymburner, L., Beggs, P., & Jacobson, C. (2000). Estimation of canopy-average surface-specific leaf area using Landsat TM data. Retrieved from http://hdl.handle.net/1959.14/1153096

Mallinis, G., & Koutsias, N. (2012). Comparing ten classification methods for burned area mapping in a Mediterranean environment using Landsat TM satellite data. *International Journal of Remote Sensing*, *33*(14), 4408–4433. https://doi.org/10.1080/01431161.2011.648284

Maselli, F. (2001). Definition of Spatially Variable Spectral Endmembers by Locally Calibrated Multivariate Regression Analyses. *Remote Sensing of Environment*, *75*(1), 29–38. https://doi.org/10.1016/S0034-4257(00)00153-X

McFeeters, S. K. (1996). The use of the Normalized Difference Water Index (NDWI) in the delineation of open water features. *International Journal of Remote Sensing*, *17*(7), 1425–1432. https://doi.org/10.1080/01431169608948714

Miller, J. D., & Thode, A. E. (2007). Quantifying burn severity in a heterogeneous landscape with a relative version of the delta Normalized Burn Ratio (dNBR). *Remote Sensing of Environment*, *109*(1), 66–80. https://doi.org/10.1016/j.rse.2006.12.006

Miller, J. D., & Yool, S. R. (2002). Mapping forest post-fire canopy consumption in several overstory types using multi-temporal Landsat TM and ETM data. *Remote Sensing of Environment*, *82*(2), 481–496. https://doi.org/10.1016/S0034-4257(02)00071-8

Mitchard, E. T. A., Saatchi, S. S., Lewis, S. L., Feldpausch, T. R., Woodhouse, I. H., Sonké, B., … Meir, P. (2011). Measuring biomass changes due to woody encroachment and deforestation/degradation in a forest–savanna boundary region of central Africa using multi-temporal L-band radar backscatter. *Remote Sensing of Environment*, *115*(11), 2861–2873. https://doi.org/10.1016/j.rse.2010.02.022

Mitchard, E. T. A., Saatchi, S. S., Woodhouse, I. H., Nangendo, G., Ribeiro, N. S., Williams, M., … Meir, P. (2009). Using satellite radar backscatter to predict above-ground woody biomass: A consistent relationship across four different African landscapes. *Geophysical Research Letters*, *36*(23), L23401. https://doi.org/10.1029/2009GL040692

Mougin, E., Proisy, C., Marty, G., Fromard, F., Puig, H., Betoulle, J. L., & Rudant, J. P. (1999). Multifrequency and multipolarization radar backscattering from mangrove forests. *IEEE Transactions on Geoscience and Remote Sensing*, *37*(1), 94–102. https://doi.org/10.1109/36.739128

Navarro, G., Caballero, I., Silva, G., Parra, P.-C., Vázquez, Á., & Caldeira, R. (2017). Evaluation of forest fire on Madeira Island using Sentinel-2A MSI imagery. *International Journal of Applied Earth Observation and Geoinformation*, *58*(Supplement C), 97–106. https://doi.org/10.1016/j.jag.2017.02.003

Ozesmi, S. L., & Bauer, M. E. (2002). Satellite remote sensing of wetlands. *Wetlands Ecology and Management*, *10*(5), 381–402. https://doi.org/10.1023/A:1020908432489

Pal, M. (2005). Random forest classifier for remote sensing classification. *International Journal of Remote Sensing*, *26*(1), 217–222. https://doi.org/10.1080/01431160412331269698

Paloscia, S., Macelloni, G., Pampaloni, P., & Sigismondi, S. (1999). The potential of C- and L-band SAR in estimating vegetation biomass: the ERS-1 and JERS-1 experiments. *IEEE Transactions on Geoscience and Remote Sensing*, *37*(4), 2107–2110. https://doi.org/10.1109/36.774723

Patterson, M. W., & Yool, S. R. (1998). Mapping Fire-Induced Vegetation Mortality Using Landsat Thematic Mapper Data. *Remote Sensing of Environment*, *65*(2), 132–142. https://doi.org/10.1016/S0034-4257(98)00018-2

Pereira, J. M. C. (1999). A comparative evaluation of NOAA/AVHRR vegetation indexes for burned surface detection and mapping. *IEEE Transactions on Geoscience and Remote Sensing*, *37*(1), 217–226. https://doi.org/10.1109/36.739156

Perry, C. R., & Lautenschlager, L. F. (1984). Functional equivalence of spectral vegetation indices. Remote Sensing of Environment, 14(1), 169–182. https://doi.org/10.1016/0034-4257(84)90013-0

Petropoulos, G. P., Knorr, W., Scholze, M., Boschetti, L., & Karantounias, G. (2010). Combining ASTER multispectral imagery analysis and support vector machines for rapid and cost-effective post-fire assessment: a case study from the Greek wildland fires of 2007. *Nat. Hazards Earth Syst. Sci.*, *10*(2), 305–317. https://doi.org/10.5194/nhess-10-305-2010

Petropoulos, George P., Kontoes, C., & Keramitsoglou, I. (2011). Burnt area delineation from a uni-temporal perspective based on Landsat TM imagery classification using Support Vector Machines. *International Journal of Applied Earth Observation and Geoinformation*, *13*(1), 70–80. https://doi.org/10.1016/j.jag.2010.06.008

Petropoulos, George P., Vadrevu, K. P., Xanthopoulos, G., Karantounias, G., & Scholze, M. (2010). A Comparison of Spectral Angle Mapper and Artificial Neural Network Classifiers Combined with Landsat TM Imagery Analysis for Obtaining Burnt Area Mapping. *Sensors*, *10*(3), 1967–1985. https://doi.org/10.3390/s100301967

Pinty, B., & Verstraete, M. (1992). GEMI: a non-linear index to monitor global vegetation from satellites. Vegetatio, 101(1), 15–20. https://doi.org/10.1007/BF00031911

Power, S., Casey, T., Folland, C., Colman, A., & Mehta, V. (1999). Inter-decadal modulation of the impact of ENSO on Australia. *Climate Dynamics*, *15*(5), 319–324. https://doi.org/10.1007/s003820050284

Pu, R., & Gong, P. (2004). Determination of burnt scars using logistic regression and neural network techniques from a single post-fire Landsat 7 ETM+ image. *Photogrammetric Engineering & Remote Sensing*, *70*(7), 841–850.

Qi, J., Chehbouni, A., Huete, A. R., Kerr, Y. H., & Sorooshian, S. (1994). A modified soil adjusted vegetation index. Remote Sensing of Environment, 48(2), 119–126. https://doi.org/10.1016/0034-4257(94)90134-1

R Core Team. (2017). *R: A language and environment for statistical computing*. Vienna, Austria: R Foundation for Statistical Computing. Retrieved from https://www.R-project.org/

Richardson, A., & Wiegand, C. (1977). Distinguishing vegetation from soil background information (by gray mapping of Landsat MSS data). Photogrammetric Engineering and Remote Sensing, 43, 1541–1522.

Rignot, E. J., Zimmermann, R., & Zyl, J. J. van. (1995). Spaceborne applications of P band imaging radars for measuring forest biomass. *IEEE Transactions on Geoscience and Remote Sensing*, *33*(5), 1162–1169. https://doi.org/10.1109/36.469480

Rodriguez-Galiano, V. F., Ghimire, B., Rogan, J., Chica-Olmo, M., & Rigol-Sanchez, J. P. (2012). An assessment of the effectiveness of a random forest classifier for land-cover classification. *ISPRS Journal of Photogrammetry and Remote Sensing*, *67*, 93–104. https://doi.org/10.1016/j.isprsjprs.2011.11.002

Rogan, J., & Franklin, J. (2001). Mapping Wildfire Burn Severity in Southern California Forests and Shrublands Using Enhanced Thematic Mapper Imagery. *Geocarto International*, *16*(4), 91–106. https://doi.org/10.1080/10106040108542218

Rouse, J. W., Haas, R. H., Scheel, J. A., & Deering, D. W. (1974). Monitoring Vegetation Systems in the Great Plains with ERTS (Vol. 1, pp. 48–62). Presented at the 3rd Earth Resource Technology Satellite (ERTS) Symposium.

Saatchi, S., Halligan, K., Despain, D. G., & Crabtree, R. L. (2007). Estimation of Forest Fuel Load From Radar Remote Sensing. *IEEE Transactions on Geoscience and Remote Sensing*, *45*(6), 1726–1740. https://doi.org/10.1109/TGRS.2006.887002

Silleos, N. G., Alexandridis, T. K., Gitas, I. Z., & Perakis, K. (2006). Vegetation Indices: Advances Made in Biomass Estimation and Vegetation Monitoring in the Last 30 Years. *Geocarto International*, *21*(4), 21–28. https://doi.org/10.1080/10106040608542399

Small, C. (2001). Estimation of urban vegetation abundance by spectral mixture analysis. *International Journal of Remote Sensing*, *22*(7), 1305–1334. https://doi.org/10.1080/01431160151144369

Stephenson, C., Handmer, J., & Betts, R. (2013). Estimating the economic, social and environmental impacts of wildfires in Australia. *Environmental Hazards*, *12*(2), 93–111. https://doi.org/10.1080/17477891.2012.703490

Stofan, E. R., Evans, D. L., Schmullius, C., Holt, B., Plaut, J. J., Zyl, J. van, … Way, J. (1995). Overview of results of Spaceborne Imaging Radar-C, X-Band Synthetic Aperture Radar (SIR-C/X-SAR). *IEEE Transactions on Geoscience and Remote Sensing*, *33*(4), 817–828. https://doi.org/10.1109/36.406668

Stroppiana, D., Azar, R., Calò, F., Pepe, A., Imperatore, P., Boschetti, M., … Lanari, R. (2015). Integration of Optical and SAR Data for Burned Area Mapping in Mediterranean Regions. *Remote Sensing*, *7*(2), 1320–1345. https://doi.org/10.3390/rs70201320

Thiam, A. K. (1998). Geographic information systems and remote sensing methods for assessing and monitoring land degradation in the Sahel region: The case of southern Mauritania. Ph.D. Thesis. Retrieved from http://adsabs.harvard.edu/abs/1998PhDT.....94T

Treuhaft, R. N., & Cloude, S. R. (1999). The structure of oriented vegetation from polarimetric interferometry. *IEEE Transactions on Geoscience and Remote Sensing*, *37*(5), 2620–2624. https://doi.org/10.1109/36.789657

United States Geological Survey (USGS). (2011, December 13). USGS EO-1. Retrieved 30 September 2017, from https://eo1.usgs.gov/sensors/hyperioncoverage

van Leeuwen, W. J. D., Huete, A. R., & Laing, T. W. (1999). MODIS Vegetation Index Compositing Approach: A Prototype with AVHRR Data. Remote Sensing of Environment, 69(3), 264–280. https://doi.org/10.1016/S0034-4257(99)00022-X

Viedma, O., Meliá, J., Segarra, D., & Garcia-Haro, J. (1997). Modeling rates of ecosystem recovery after fires by using landsat TM data. *Remote Sensing of Environment*, *61*(3), 383–398. https://doi.org/10.1016/S0034-4257(97)00048-5

Xu, H. (2006). Modification of normalised difference water index (NDWI) to enhance open water features in remotely sensed imagery. *International Journal of Remote Sensing*, *27*(14), 3025–3033. https://doi.org/10.1080/01431160600589179

Yang, X., & Lo, C. P. (2002). Using a time series of satellite imagery to detect land use and land cover changes in the Atlanta, Georgia metropolitan area. *International Journal of Remote Sensing*, *23*(9)

Appendix

Appendix 1: Accuracy results of Random Forest Classifiers.

Carinda Rd

	8/03/16	24/03/16	25/04/16	11/05/16	27/05/16	Average	ST.DEV
Training Accuracy	0.9920	0.9913	0.9741	0.9930	0.9927	0.9886	0.0073
Training Kappa Value	0.9940	0.9896	0.9690	0.9916	0.9912	0.9871	0.0092
Validation Accuracy	0.9193	0.9152	0.4842	0.5951	0.4179	0.6663	0.2126
95% CI	0.9117, 0.9264	0.9075, 0.9225	0.4709, 0.4975	0.582, 0.6082	0.4048, 0.4311	N/A	N/A
No Info Rate	0.1841	0.184	0.184	0.184	0.184	N/A	N/A
P-Value (Acc > NIR)	< 2.2e-16	< 2.2e-16	< 2.2e-16	< 2.2e-16	< 2.2e-16	N/A	N/A
Overall Kappa Value	0.9017	0.8977	0.9026	0.5088	0.3235	0.7069	0.2445

Masmans

	29/10/14	1/01/15	17/01/15	2/02/15	18/02/15	6/03/15	Average	ST.DEV
Training Accuracy	0.9766	0.9814	0.9813	0.9800	0.9820	0.9730	0.9766	0.0032
Training Kappa Value	0.9715	0.9775	0.9773	0.9757	0.9673	0.9673	0.9715	0.0044
Validation Accuracy	0.7244	0.6381	0.7054	0.6126	0.5087	0.5741	0.7244	0.0739
95% CI	0.7122, 0.7364	0.6521, 0.6509	0.693, 0.7176	0.5994, 0.6256	0.4953, 0.5222	0.5607, 0.5873	0.7122, 0.7364	N/A
No Info Rate	0.1881	0.1865	0.1865	0.1865	0.1865	0.1865	0.1881	N/A
P-Value (Acc > NIR)	< 2.2e-16	< 2.2e-16	< 2.2e-16	< 2.2e-16	< 2.2e-16	< 2.2e-16	< 2.2e-16	N/A
Overall Kappa Value	0.6717	0.5621	0.6253	0.5423	0.3977	0.4942	0.6717	0.0885

Cresswell

	2/02/15	6/03/15	23/04/15	9/05/15	Average	ST.DEV
Training Accuracy	0.9779	0.9727	0.9779	0.9659	0.9736	0.0049
Training Kappa Value	0.9731	0.9673	0.9731	0.9591	0.9681	0.0057
Validation Accuracy	0.6289	0.6311	0.6289	0.5837	0.6182	0.0199
95% CI	0.6157, 0.6419	0.6181, 0.6438	0.6157, 0.6419	0.5706, 0.5968	N/A	N/A
No Info Rate	0.1881	0.1824	0.1824	0.1824	N/A	N/A
P-Value (Acc > NIR)	< 2.2e-16	< 2.2e-16	< 2.2e-16	< 2.2e-16	N/A	N/A
Overall Kappa Value	0.5599	0.5654	0.3755	0.4972	0.4995	0.0764

Appendix 1 cont.

Individual Class Accuracy Results

Carinda Rd

Class	8/03/16	24/03/16	25/04/16	11/05/16	27/05/16	Average
Inundated Vegetation	0.9586	N/A	N/A	N/A	N/A	0.9586
River or Stream	0.7439	0.8714	0.7751	0.7305	0.5513	0.7344
Paddock or Field	0.9994	0.9554	0.9875	0.9553	0.9817	0.9759
Wetland Marsh	0.9336	0.8546	0.9228	0.6165	0.5078	0.7671
Open Water or Basin	1.0000	1.0000	0.9915	0.6579	0.4995	0.8298
Sclerophyll Woodland	0.9539	0.9451	0.9311	0.6487	0.4907	0.7939
Burned	N/A	1.0000	0.9998	0.9052	0.9218	0.9567

Cresswell

Class	2/02/15	6/03/15	23/04/15	9/05/15	Average
Burned	N/A	0.9991	1.0000	1.0000	0.9997
Dryland Vegetation	0.9465	0.8965	0.9555	0.9162	0.9287
Field or Paddock	0.9743	0.8685	0.8678	0.8687	0.8948
Open Plain or Grassland	0.5764	0.8128	0.4964	0.8226	0.6771
River or Stream	0.8870	0.7010	0.4845	0.4927	0.6413
Sclerophyll Woodland	0.4117	0.4655	0.3660	0.4732	0.4291
Wetland Marsh/Inundated	0.9937	0.9242	0.7621	0.7048	0.8462

Masmans

Class	29/10/14	1/01/15	17/01/15	2/02/15	18/02/15	6/03/15	Average
Burned	N/A	0.9996	0.9880	0.9990	0.9833	0.9996	0.9939
Dryland Vegetation	0.9107	0.9730	0.9432	0.9117	0.6950	0.9087	0.8904
Field or Paddock	0.9316	0.9153	0.8867	0.9751	0.9658	0.8776	0.9254
Open Plain or Grassland	0.9583	0.6797	0.9664	0.5524	0.5754	0.6254	0.7263
River or Stream	0.7190	0.8156	0.6351	0.8957	0.4999	0.6870	0.7087
Sclerophyll Woodland	0.4987	0.4434	0.5038	0.4068	0.4406	0.4182	0.4519
Wetland Marsh/Inundated	0.9661	0.8750	0.9449	0.9920	0.8652	0.9449	0.9314

Appendix 1 cont.

Random Forest Classification Validation Confusion Matrices

Mid-fire classification. Columns are reference, rows are prediction.

Carinda Rd

	Sclerophyll Forest	Burned	Open Water or Basin	Paddock or Field	River or Stream	Wetland Marsh
Sclerophyll Forest	905	0	0	0	66	0
Burned	0	1001	0	0	0	0
Open Water or Basin	0	0	0	0	0	0
Paddock or Field	2	0	0	1001	0	33
River or Stream	61	0	0	0	350	248
Wetland Marsh	32	0	0	0	13	720

Cresswell

	Sclerophyll Forest	Open Plain or Grassland	Burned	Dryland Vegetation	Field or Paddock	River or Stream	Wetland Marsh
Sclerophyll Forest	5	331	0	1	0	1	0
Open Plain or Grassland	0	653	0	119	1	0	0
Burned	0	0	167	0	0	10	0
Dryland Vegetation	0	17	0	820	104	0	0
Field or Paddock	0	0	0	3	679	0	0
River or Stream	929	0	0	1	0	191	49
Wetland Marsh	66	0	0	56	218	121	952

Masmans

	Sclerophyll Forest	Open Plain or Grassland	Burned	Dryland Vegetation	Field or Paddock	River or Stream	Wetland Marsh
Sclerophyll Forest	5	517	0	0	0	0	0
Open Plain or Grassland	44	386	0	3	68	0	0
Burned	0	0	47	4	0	0	
Dryland Vegetation	0	44	0	979	100	0	0
Field or Paddock	0	0	0	8	834	0	0
River or Stream	204	5	0	0	0	203	43
Wetland Marsh	747	49	0	6	0	103	958

Appendix 2: Commission and omission error rates of each classifier by fire event.

Neural Networks

Carinda Rd	Commission Error Rate (%)	Omission Error Rate (%)
Mid-fire	0.14%	23.91%
1st Post-fire	0.69%	29.85%
2nd Post-fire	26.67%	49.29%
3rd Post-fire	28.39%	38.67%
Average	**13.97%**	**35.43%**
Cresswell		
Mid-fire	4.97%	83.31%
1st Post-fire	100.00%	100.00%
2nd Post-fire	0.00%	87.81%
Average	**34.99%**	**90.37%**
Masmans		
Mid-fire	0.00%	0.00%
1st Post-fire	0.00%	0.00%
2nd Post-fire	0.00%	0.00%
3rd Post-fire	0.00%	0.00%
4th Post-fire	0.00%	0.00%
Average	**0.00%**	**0.00%**

Random Forest

Carinda Rd	Commission Error Rate (%)	Omission Error Rate (%)
Mid-fire	0.01%	68.19%
1st Post-fire	0.00%	67.38%
2nd Post-fire	0.00%	62.86%
3rd Post-fire	0.24%	58.61%
Average	**0.06%**	**64.26%**
Cresswell		
Mid-fire	0.97%	59.17%
1st Post-fire	0.10%	76.87%
2nd Post-fire	0.00%	72.42%
Average	**0.36%**	**69.49%**
Masmans		
Mid-fire	100.00%	100.00%
1st Post-fire	98.80%	19.19%
2nd Post-fire	98.63%	17.44%
3rd Post-fire	97.24%	15.12%
4th Post-fire	99.28%	18.02%
Average	**98.79%**	**33.95%**

Appendix 2 cont.

Support Vector Machine

Carinda Rd	Commission Error Rate (%)	Omission Error Rate (%)
Mid-fire	0.05%	25.01%
1st Post-fire	0.04%	34.77%
2nd Post-fire	4.10%	43.55%
3rd Post-fire	9.14%	35.90%
Average	**3.33%**	**34.81%**
Cresswell		
Mid-fire	3.03%	49.50%
1st Post-fire	4.16%	71.19%
2nd Post-fire	0.86%	70.25%
Average	**2.68%**	**63.65%**
Masmans		
Mid-fire	71.72%	12.21%
1st Post-fire	99.59%	4.65%
2nd Post-fire	99.10%	100.00%
3rd Post-fire	99.65%	7.56%
4th Post-fire	99.51%	9.30%
Average	**93.91%**	**26.74%**

Appendix 3: Three-minute thesis poster submission for Wetlands in Drylands (WiDs) 2017 conference.

A Comparative Analysis of Classification Methods for Burn Scar Mapping in Wetlands

WIDS2017 Wetlands in Drylands Research Network Conference

Macquarie University • 24-26th July 2017
wetlandsindrylands.net • #WIDS2017MQ

Poster number
Leave this
space blank

Mackenzie L. C. Austin[1], Hsing-Chung Chang[1], Kerrie M. Tomkins[1], Timothy J. Ralph[1]

Introduction:

- Fire has a profound impact on wetland environments, with typically negative consequences including habitat loss and irreparable damage to biodiversity.
- Understanding the behaviour of these fires, particular their intensity and spatial extent, is key in informing management practices
- Field studies for these vast and remote areas are often costly and inefficient in terms of area covered.
- Remote sensing methods provide an alternative that can cover far greater spatial areas with increased temporal frequency and spectral resolution.

Site Area:

- The study is focused on wetlands in drylands, with a focus on the Macquarie Marshes and Gwydir Wetlands.
- Five particular fire events are being analysed:

Fire Name	Origin	Start Date	End Date	Duration	Area (Ha)	Perimeter (KM)
Carinda Rd, The Marra	Wildfire	15/03/16	26/03/16	11 days	3308.932	30.843
Ninia	Prescribed burn	31/03/15	1/04/15	2 days	372.636	8.132
North Marsh Cresswell	Wildfire	1/03/15	14/03/15	13 days	176.440	5.708
Macquarie Marshes Cresswell	Wildfire	25/02/15	14/03/15	21 days	206.588	7.213
Masmans	Wildfire	29/12/14	6/01/15	8 days	15.358	1.887

Methods:

- The first stage of the study was to acquire the data, which consisted of primarily Landsat 8 imagery which was then radiometrically and atmospherically calibrated.
- The methodology consists of two major components:
  - calculating spectral indices such as the NDVI, NBR, and others
  - performing unsupervised and supervised classifications on satellite imagery
- The spectral indices calculated use the visible and infrared segments of the ER spectrum to analyse vegetation cover and delineate burned pixels (rapid land cover change). The results of these can be observed in Figure 2.
- The unsupervised classification method used is K-Means, which is compared to the supervised options of Random Forest, Neural Networks, and Support Vector Machines. The results of these can be observed below in Figure 3.

Results and Implications:

- Supervised classification methods are proving to be far more accurate than unsupervised methods, delineating vegetated and burned areas with greater detail.
- This will allow greater insights into the characteristics of bushfires in wetland areas and how they behave over their active period, and inform management efforts and allow better responses to bushfire events.

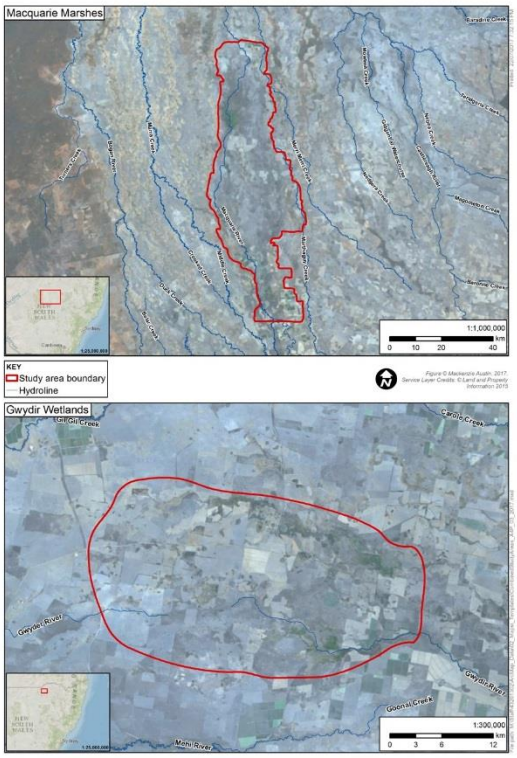

Figure 1: Map of study areas.

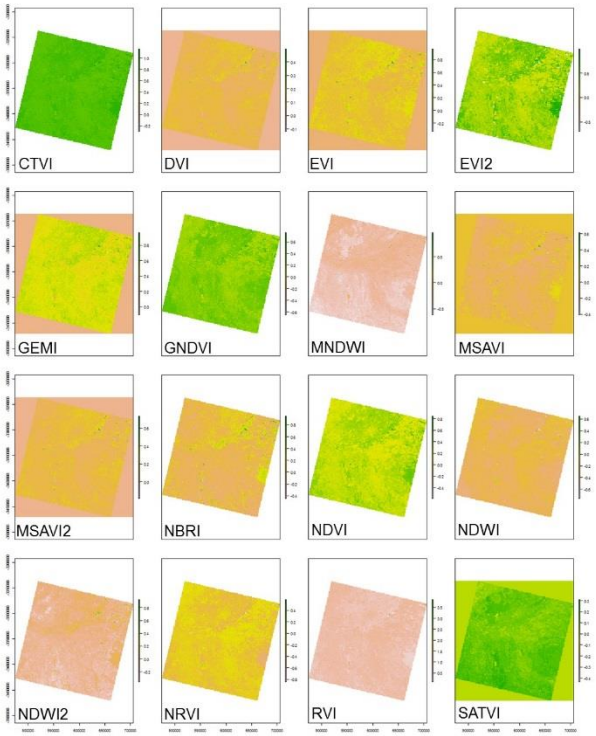

Figure 2: Visual comparison of different spectral indices on pre-burn wetland vegetation in the Macquarie Marshes.

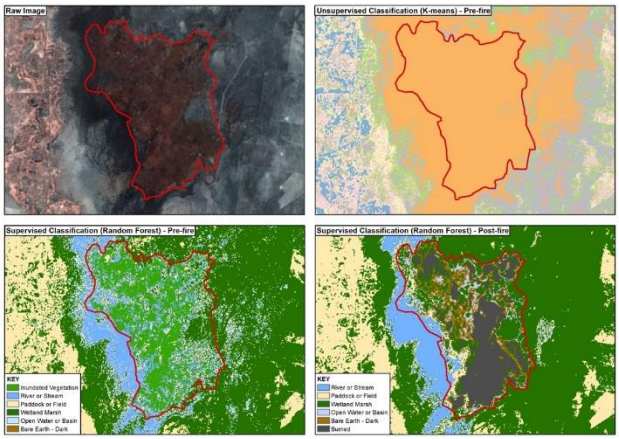

Figure 3: Comparison of classification methods on imagery covering Macquarie Marshes.

MACQUARIE University

[1]Department of Environmental Sciences, Macquarie University, NSW 2109, Australia. Email mackenzie.austin@hdr.mq.edu.au, michael.chang@mq.edu.au., kerrie.tomkins@mq.edu.au, tim.ralph@mq.edu.au.

Appendix 4: WiDs 2017 conference abstract.

A Comparative Analysis of Classification Methods for Burn Scar Mapping in Wetlands

Mackenzie L. C. Austin[1], Hsing-Chung Chang[1], Kerrie M. Tomkins[1], Timothy J. Ralph[1]

This project explores the role and history of fire in the Macquarie Marshes and Gwydir Wetlands (NSW) with two key objectives; to compare the spectral indices and classification methods that can be utilised for burn scar mapping, and to understand the behaviour of vegetation regeneration and regrowth in post-fire wetland ecosystems, namely the rate of regeneration and its relation to variables influencing burn severity, such as wetland moisture content. The methodology consists of multiple stages, the first of which includes performing spectral indices such as the normalised vegetation differential index (NDVI) and NDVI-Difference, burned area index (BAI), and the leaf area index (LAI) using satellite imagery. These processes measure the red and near-infrared light reflected from a sensed surface, which can be used to calculate green vegetation cover and density, which will allow for the detection of the large vegetation losses caused by bushfires. These outputs will then be classified by different classification methods such as neural networks (NNs), support vector machine (SVM) and random forest (RF) to determine the accuracy of the delineation between ‘burned’ and ‘unburned’ pixels, with a comparative statistical analysis performed to ensure accurate results. Finally, these outputs will be sequenced to form a time-series analysis, highlighting vegetation regeneration over time.

Appendix 5: Index of sensors and their characteristics.

	Landsat 8 OLI/TIRS[1]	Landsat 7 ETM+[2]	Landsat 4/5 TM[3]	MODIS[4]	Sentinel-2A/B[5]
Mission Dates	February 2013 - Current	April 1999 - Current	July 1982 - May 2012	December 1999 - Current	June 2015 - Current
Sensor Type/s	Operational Land Imager, Thermal Infrared Sensor	Enhanced Thematic Mapper Plus	Thematic Mapper, Multispectral Scanner	Moderate Resolution Imaging Spectroradiometer	Multispectral Instrument (MSI) including VNIR and SWIR
Bands	1 - 11	1 - 8	1 - 7	1 - 36	1 - 12
Spectral Range (Wavelength - µm)	Band 1: 0.43-0.45 (Coastal Aerosol)	Band 1: 0.45-0.52 (Blue)	TM:	Band 1: 0.62-0.67 (Absolute Land Cover Transformation, Vegetation Chlorophyll)	Band 1: 0.443 (Coastal Aerosol)
	Band 2: 0.45-0.51 (Blue)	Band 2: 0.52-0.60 (Green)	Band 1: 0.45-0.52 (Blue)	Band 2: 0.841-0.876 (Cloud Amount, Vegetation Land Cover Transformation)	Band 2: 0.490 (Blue)
	Band 3: 0.53-0.59 (Green)	Band 3: 0.63-0.69 (Red)	Band 2: 0.52-0.60 (Green)	Band 3: 0.459-0.479 (Soil Vegetation Differences)	Band 3: 0.560 (Green)
	Band 4: 0.64-0.67 (Red)	Band 4: 0.76-0.90 (NIR)	Band 3: 0.63-0.69 (Red)	Band 4: 0.545-0.565 (Green Vegetation)	Band 4: 0.665 (Red)
	Band 5: 0.85-0.88 (NIR)	Band 5: 1.55-1.75 (NIR)	Band 4: 0.76-0.90 (NIR)	Band 5: 1.230-1.250 (Leaf/Canopy Differences)	Band 5: 0.705 (Vegetation Red Edge)
	Band 6: 1.57-1.65 (SWIR-1)	Band 6: 10.40-12.50 (TIR)	Band 5: 1.55-1.75 (NIR)	Band 6: 1.628-1.652 (Snow/Cloud Differences)	Band 6: 0.740 (Vegetation Red Edge)
	Band 7: 2.11-2.29 (SWIR-2)	Band 7: 2.08-2.35 (MIR)	Band 6: 10.40-12.50 (TIR)	Band 7: 2.105-2.155 (Cloud Properties, Land Properties)	Band 7: 0.783 (Vegetation Red Edge)
	Band 8: 0.50-0.68 (Panchromatic)	Band 8: 0.52 - 0.90 (Panchromatic)	Band 7: 2.08-2.35 (MIR)	Band 8: 0.405-0.42 (Chlorophyll)	Band 8: 0.842 (NIR)
	Band 9: 1.36-1.38 (Cirrus)			Band 9: 0.438-0.448 (Chlorophyll)	Band 8A: 0.865 (Vegetation Red Edge)
	Band 10: 10.60-11.19 (TIRS-1)		MSS:	Band 10: 0.483-0.493 (Chlorophyll)	Band 9: 0.945 (Water Vapour)
	Band 11: 11.50-12.51 (TIRS-2)		Band 4: 0.5-0.6 (Green)	Band 11: 0.526-0.536 (Chlorophyll)	Band 10: 1.375 (SWIR - Cirrus)
			Band 5: 0.6-0.7 (Red)	Band 12: 0.546-0.556 (Atmosphere, Sediments)	Band 11: 1.610 (SWIR)
			Band 6: 0.7-0.8 (NIR)	Band 13: 0.662-0.672 (Atmosphere, Sediments)	Band 12: 2.190 (SWIR)
			Band 7: 0.8-1.1 (NIR)	Band 14: 0.673-0.683 (Chlorophyll Fluorescence)	
				Band 15: 0.743-0.753 (Aerosol Properties)	
				Band 16: 0.862-0.877 (Aerosol Properties, Atmospheric Properties)	
				Band 17: 0.890-0.920 (Atmospheric Properties, Cloud Properties)	
				Band 18: 0.931-0.941 (Atmospheric Properties, Cloud Properties)	
				Band 19: 0.915-0.965 (Atmospheric Properties, Cloud Properties)	
				Band 20: 3.660-3.840 (Sea Surface Temperature)	
				Band 21: 3.929-3.989 (Forest Fires & Volcanoes)	
				Band 22: 3.929-3.989 (Cloud Temperature, Surface Temperature)	
				Band 23: 4.020-4.080 (Cloud Temperature, Surface Temperature)	
				Band 24: 4.433-4.498 (Cloud Fraction, Troposphere Temperature)	
				Band 25: 4.482-4.549 (Cloud Fraction, Troposphere Temperature)	
				Band 26: 1.36-1.39 (Cloud Fraction - Thin Cirrus, Troposphere Temperature)	
				Band 27: 6.535-6.895 (Mid Troposphere Humidity)	
				Band 28: 7.175-7.475 (Upper Troposphere Humidity)	
				Band 29: 8.4-8.7 (Surface Temperature)	
				Band 30: 9.58-9.88 (Total Ozone)	
				Band 31: 10.78-11.28 (Cloud Temperature, Forest Fires & Volcanoes, Surface Temperature)	
				Band 32: 11.77-12.27 (Cloud Height, Forest Fires & Volcanoes, Surface Temperature)	
				Band 33: 13.185-13.485 (Cloud Fraction, Cloud Height)	
				Band 34: 13.485-13.785 (Cloud Fraction, Cloud Height)	
				Band 35: 13.785-14.085 (Cloud Fraction, Cloud Height)	
				Band 36: 14.085-14.385 (Cloud Fraction, Cloud Height)	
Spatial Resolution	30m (Bands 1-7, 9), 15m (Band 8), 100m (Bands 10-11)*	30m (Bands 1-5, 7), 60m (Band 6)*, 15m (Band 8)	TM: 30m (Bands 1-5, 7), 120m (Band 6)* MSS: 57m	250m (Bands 1-2), 500m (Bands 3-7), 1000m (Bands 8-36)	60m (Band 1, 9-10), 10m (Band 2-4, 8), 20m (Band 5-7, 8A, 11-12)
Swath Width	185km	185km	185km	2300km	290km
Regime	Polar, Sun-synchronous	Polar, Sun-synchronous	Near-polar, Sun-synchronous	Sun-synchronous, Low Earth, Near-polar	Sun-synchronous
Repeat Interval	16 days	16 days	16 days	1-2 days	5 days

*Resampled to 30m in product releases.

[1]Operational Land Imager/Thermal InfraRed Sensor

[2]Enhanced Thematic Mapper Plus

[3]Thematic Mapper

[4]Moderate-Resolution Imaging Spectroradiometer

[5]2A launched, 2B in progress